

RESEARCH ARTICLE

Escaping blood-fed malaria mosquitoes minimize tactile detection without compromising on take-off speed

F. T. Muijres^{1,*}, S. W. Chang², W. G. van Veen¹, J. Spitzen³, B. T. Biemans¹, M. A. R. Koehl² and R. Dudley²

ABSTRACT

To escape after taking a blood meal, a mosquito must exert forces sufficiently high to take off when carrying a load roughly equal to its body weight, while simultaneously avoiding detection by minimizing tactile signals exerted on the host's skin. We studied this trade-off between escape speed and stealth in the malaria mosquito *Anopheles coluzzii* using 3D motion analysis of high-speed stereoscopic videos of mosquito take-offs and aerodynamic modeling. We found that during the push-off phase, mosquitoes enhanced take-off speed using aerodynamic forces generated by the beating wings in addition to leg-based push-off forces, whereby wing forces contributed 61% of the total push-off force. Exchanging leg-derived push-off forces for wing-derived aerodynamic forces allows the animal to reduce peak force production on the host's skin. By slowly extending their long legs throughout the push-off, mosquitoes spread push-off forces over a longer time window than insects with short legs, thereby further reducing peak leg forces. Using this specialized take-off behavior, mosquitoes are capable of reaching take-off speeds comparable to those of similarly sized fruit flies, but with weight-normalized peak leg forces that were only 27% of those of the fruit flies. By limiting peak leg forces, mosquitoes possibly reduce the chance of being detected by the host. The resulting combination of high take-off speed and low tactile signals on the host might help increase the mosquito's success in escaping from blood-hosts, which consequently also increases the chance of transmitting vector-borne diseases, such as malaria, to future hosts.

KEY WORDS: Biomechanics, Aerodynamics, Insect, Flight behavior, Take-off maneuvers, Wingbeat kinematics

INTRODUCTION

To reproduce, a gravid female malaria mosquito needs a blood meal for egg development (Clements, 2011). To acquire this meal, the mosquito must approach a host, feed, and then escape without being detected. Host searching and the bite dynamics of malaria mosquitoes have been well studied (Clements, 2011; Krenn and Aspöck, 2012; Takken, 1991), but little is known about the escape dynamics of blood-feeding insects (Roitberg et al., 2003).

A robust strategy for a mosquito to successfully escape from a host would simultaneously comprise a sufficiently high escape speed and a low chance of being detected. Escape speed and consequent

survival of blood-fed mosquitoes scale inversely with meal size (Roitberg et al., 2003), thus escape performance is constrained by the blood load carried. Blood loads in fed mosquitoes can double to triple the animals' total weight (Roitberg et al., 2003), and thus despite their reduced escape speed, blood-fed mosquitoes are expected to generate higher push-off forces than unfed individuals. This outcome might increase tactile signaling to the host, potentially reducing mosquito survivability, and consequently the chance that the mosquito transmits pathogens (such as *Plasmodium* parasites) to future hosts (Takken and Knols, 1999). Mechanosensory hairs of mammals have a mechanical load detection threshold of less than 0.07 mN (Li et al., 2011). This threshold was determined using the von Frey assay, whereby nylon threads with varying thickness are used to test a rodent's sensitivity to mechanical stimulation (Mogil et al., 2001). This type of stimulus can be expected to be similar to the push-off forces produced by the legs of an escaping insect. Therefore, a hematophagous animal escaping from a mammalian host could avoid detection by exerting ground reaction forces below the detection threshold of 0.07 mN. However, such reduction in push-off forces might lead to a decrease in take-off speed, suggesting that there is a trade-off between stealth and speed in post-feeding escape take-offs of hematophagous insects.


Fruit flies, which, like mosquitoes, belong to the order Diptera and are similar in mass, use two distinct take-off maneuvers that are controlled by different neural pathways: (1) a slow voluntary take-off and (2) a fast escape in response to looming stimuli (Card and Dickinson, 2008b). During slow voluntary take-offs, the fly combines leg-derived push-off forces with wing-derived aerodynamic forces. In contrast, during the fast escape, all forces produced during the initial push-off phase are generated by the middle pair of legs, which are powered by a large specialized tergal depressor of the trochanter (TDT) muscle; no wing motion is involved (Card and Dickinson, 2008b). Unlike fruit flies, blood-feeding tsetse flies do not possess this TDT muscle, suggesting that escaping tsetse flies cannot produce the high leg forces found in fruit flies (King, 1983). Blood-feeders such as mosquitoes and tsetse flies might thus reduce the tactile signals transmitted to the skin of their host by exerting low leg push-off forces.

Mosquitoes differ from fruit flies and tsetse flies in two important ways that might affect take-off performance: (1) mosquitoes, like other culicids, generally have longer legs than other flies, and (2) mosquitoes use strikingly different wingbeat kinematics than flies. A recent study on the flight dynamics and aerodynamics of *Culex* mosquitoes (Bomphrey et al., 2017) showed that mosquitoes operate at extremely low wingbeat amplitudes (~40 deg) and high wingbeat frequencies (~700 Hz). To achieve this, mosquitoes make use of specialized aerodynamic mechanisms controlled by spanwise wing rotations, but the functional reason for using these extreme wingbeat kinematics is unknown (Bomphrey et al., 2017).

Honeybees, which need to be able to carry large nectar and pollen loads, also use wing kinematics with relatively low stroke amplitudes and high wingbeat frequencies (Altshuler et al., 2005).

¹Experimental Zoology Group, Wageningen University & Research, PO Box 338, 6700 AH, Wageningen, The Netherlands. ²Department of Integrative Biology, University of California, Berkeley, CA 94720, USA. ³Laboratory of Entomology, Wageningen University & Research, PO Box 16, 6700 AA, Wageningen, The Netherlands.

*Author for correspondence (florian.muijres@wur.nl)

 F.T.M., 0000-0002-5668-0653

These kinematics have been shown to be aerodynamically less efficient than the more conventional low-frequency, high-amplitude kinematics typical of fruit flies, but may be related to the large load-carrying capacity required of honeybees (Altshuler et al., 2005), and possibly of mosquitoes.

We examine here the take-off and flight dynamics of unfed and blood-fed malaria mosquitoes, *Anopheles coluzzii* Coetzee & Wilkerson, to determine how flying mosquitoes are capable of taking off while carrying such high blood loads, and what the potential trade-off might be between escape stealth and speed when taking off from a blood host. Using a stereoscopic high-speed camera system (Fig. 1A) we filmed the take-off dynamics of 63 malaria mosquitoes (Fig. 2, Movies 1–4), and using computational models we estimated their leg push-off dynamics and wingbeat-based aerodynamics. From μ CT scans of the thorax of a female mosquito, we also reconstructed the 3D morphology of the legs and flight power muscles (Fig. 1D). Comparing these results with data from fruit flies (Card and Dickinson, 2008a,b) shows that throughout the take-off mosquitoes produce tactile forces on the substrate that are much lower than those produced by fruit flies. In contrast, take-off speeds are surprisingly similar between the mosquitoes and fruit flies. This suggests that mosquitoes have optimized their take-off dynamics to balance the stealth and speed requirements of post-ingestion escape.

MATERIALS AND METHODS

Experimental animal

Experiments were performed on 5- to 10-day-old female malaria mosquitoes, *A. coluzzii*, from a laboratory stock kept at Wageningen University, The Netherlands. The colony originates from Liberia in

1987, and are being reared on blood obtained from the blood bank (Sanquin, The Netherlands) using a Hemotek membrane feeding system (Discovery Workshops, Accrington, UK). Because malaria mosquitoes are nocturnally active, they were reared in a clock-shifted 12 h:12 h light:dark cycle, and experiments were performed during the late-night period of the mosquitoes, which coincided with morning office hours. Prior to the experiments, a subset of mosquitoes was blood-fed on a human arm or a Hemotek membrane feeding system. Mosquitoes were then placed in custom storage containers made from a silicone tube and gauze. After an acclimatization period of 10–60 min, the take-off experiments were performed. We only used female mosquitoes that did not receive a blood meal prior to the experiments, and were therefore free of malaria parasites (Clements, 2011). For this reason, the Medical Research Ethics Committee of Wageningen University concluded that our experimental procedure did not require ethical approval according to the Dutch ‘Medical Research Involving Human Subjects Act’.

Experimental setup and procedure

The experimental setup (Fig. 1A) consisted of a rectangular enclosure (20×20×30 cm, width×depth×height) with transparent acrylic walls. At one corner of the arena was positioned a transparent horizontal take-off platform (3×1 cm, width×length), and on the opposite corner a damp black cloth functioned as a shelter for the mosquitoes within the brightly lit flight chamber. A single mosquito was placed on the platform directly from its storage container, after which it would take off and fly towards the shelter, land and rest.

Because we wanted to compare dynamics of voluntary take-offs and elicited escapes, we tried various types of stimuli to trigger

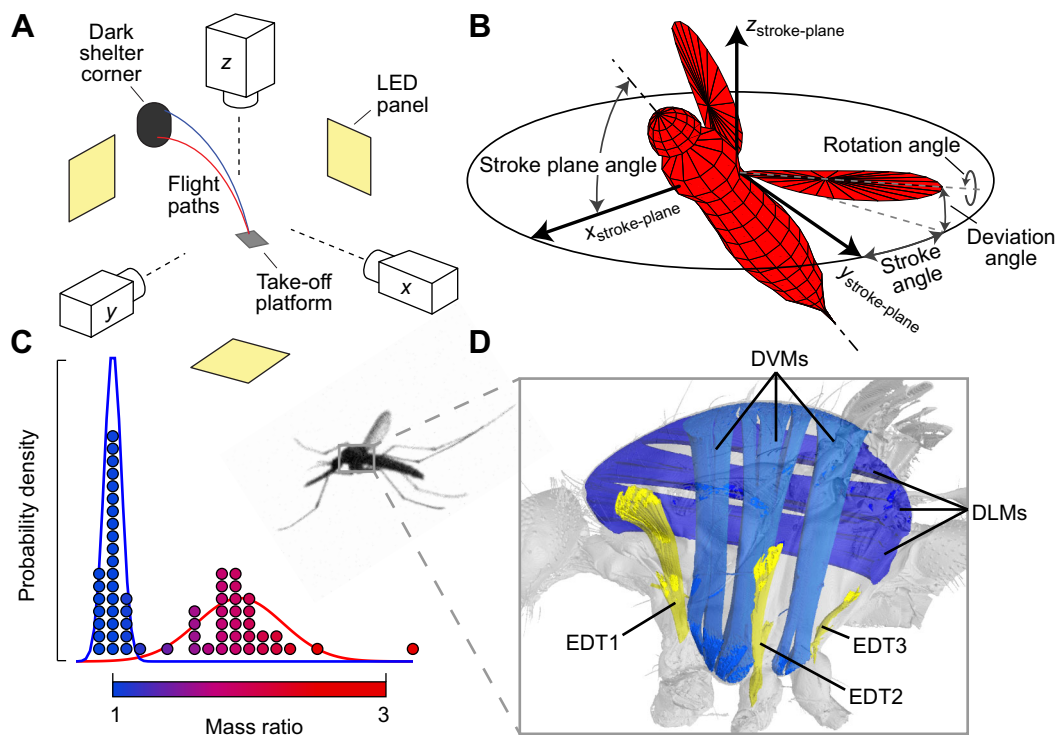


Fig. 1. Experimental setup, and morphological and kinematic characteristics of the experimental mosquitoes. (A) Experimental setup consisting of three backlit high-speed cameras (Photron Fastcam SA-X2 operating at 13,500 frames s^{-1}), and a flight arena with take-off platform and dark shelter for landing. (B) Wingbeat kinematics are defined as three Euler angles within the stroke-plane reference frame: the stroke angle, deviation angle and wing rotation angle. The stroke plane was fixed relative to the longitudinal body axis at a pitch-down angle of 47.5 deg. (C) Body mass ratio for all studied mosquitoes (Eqn 3). Lines indicate probability densities for all unfed (blue) and blood-fed (red) mosquitoes. (D) μ CT reconstruction of the dorso-ventral and dorso-longitudinal flight power muscles (DVMs and DLMs, respectively), and the extracoxal depressor muscles of the trochanter of the front, middle and hind leg (EDT1, EDT2 and EDT3, respectively).

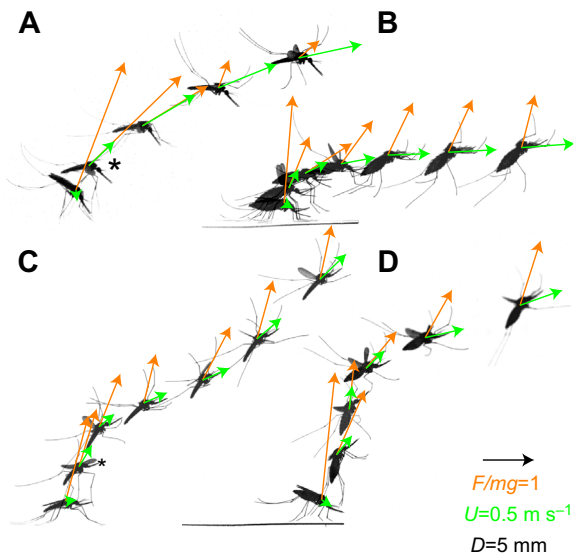


Fig. 2. Photomontages of mosquito take-offs. (A,C) Two unfed mosquitoes; (B,D) two blood-fed mosquitoes. The time step between consecutive images were 116 ms (A,B) and 32 ms (C,D). Asterisks in A and C indicate the moment of lift-off. Overlaid on each mosquito image are vectors of normalized force (orange) and velocity (green), as scaled according to the black vector in D.

escape take-offs. In sharp contrast to fruit flies (Card and Dickinson, 2008b), visual looming stimuli did not robustly trigger escape responses in these mosquitoes, possibly because malaria mosquitoes are active at night, when visual cues may not be as important for detecting danger as they are for insects active during daylight (Takken, 1991). Also, the fact that we used white lights to illuminate the experimental setup might have negatively affected the response dynamics of the mosquitoes to visual stimuli. By contrast, manually tapping the take-off platform with the silicone storage container reliably triggered take-off responses, suggesting that the mosquitoes respond more robustly to substratum vibrations than to visual looming stimuli. Therefore, we used only the tapping technique to trigger escape responses.

When a mosquito took off voluntarily or in response to platform vibrations, we manually triggered a high-speed stereoscopic video recording system to film the maneuver. The recording system consisted of three gray-scale (12 bits) high-speed cameras (Photon Fastcam SA-X2 with Nikkor Micro 200 m AF f/4D lenses at aperture F11), operating at a frame rate of $13,500 \text{ frames s}^{-1}$, an exposure time of $1/13,688 \text{ s}$ and an image resolution of 1024×1000 pixels. The experimental arena was backlit using LED panels (36 W, $300 \times 300 \text{ m}$, white light CCT 5000–5500 K) such that the mosquitoes were visualized as a dark shadow in front of a bright background. The LED panels increase the temperature in the enclosure, and therefore we used an air conditioning system to blow cooled air around the outside of the flight arena to cool the air inside to $28.5 \pm 1.08^\circ\text{C}$ (mean \pm s.d.). During experiments, cameras continuously recorded in end-trigger mode, until the manually triggered signal prompted each camera to store 1.66 s of video data prior to the trigger point. After each experiment, the mosquito was collected and killed.

Experiments were performed for 10 consecutive working days. At the start of each experimental day, the camera system was calibrated by imaging a $70 \times 70 \text{ mm}$ checkerboard calibration plate (square size 5 mm) placed at two known positions in the field of view of all cameras. Based on these images, we then used a direct linear transformation method for stereoscopic camera calibration (Hatze, 1988).

Body mass estimation

We estimated body mass of each experimental animal (blood-fed and unfed) based on their thoraco-abdominal longitudinal length and maximum abdominal width, which we estimated from the videography images. For this, we first correlated body dimensions with body mass based on a separate set of measurements on 44 female malaria mosquitoes from the same population as the experimental animals. Each mosquito was placed in a rectangular test tube, photographed from the dorsal view and weighed using an analytical balance (Mettler Toledo AG204). We then blood-fed the same mosquito and repeated the size and mass measurements.

From each photograph, we measured the longitudinal length of the thorax plus abdomen (l) and the maximum abdomen width (w), whereby image pixel size was calibrated based on the known size of the test tube. From these measurements, we calculated the volumetric parameter:

$$V_{\text{cylinder}} = \pi w^2 l / 4, \quad (1)$$

which represents a cylindrical volume with length equal to the thoraco-abdominal length l and diameter equal to the maximum abdominal width w . Body mass m (in mg) was then correlated with V_{cylinder} (in mm^3) using the linear fit (Fig. S1):

$$m = a(V_{\text{cylinder}}) + b, \quad (2)$$

whereby a and b are the linear fit coefficients [$a=0.501$ (0.447 0.555); $b=0.827$ (0.680 0.973), mean (95% confidence interval), $r^2=0.826$]. This fit was used to estimate body mass from measured body dimensions in our experiments.

For every take-off sequence, we selected a top-view video image in which the mosquito body was positioned as horizontally as possible. This video image was then calibrated using the corresponding image of the calibration checkerboard, after which the mosquito's thoraco-abdominal longitudinal length l and maximum abdominal width w were determined. From these measurements, we estimated body mass using the aforementioned linear fit between cylindrical volume and body mass (Fig. S1, Fig. 1C). We then determined the animal's mass ratio as:

$$R_m = m / m_{\text{unfed}}, \quad (3)$$

where m_{unfed} is the mean mass of all unfed experimental mosquitoes.

Analyzing body and wing movements throughout the take-off

We used a combination of automatic and manual tracking to determine body and wingbeat kinematics throughout the take-off maneuvers of blood-fed and unfed mosquitoes. The automatic tracker was an adaptation of a machine-vision-based tracker developed for studying flight dynamics of fruit flies (Fontaine et al., 2009). For this adaptation, we developed a new wing geometry model, a new wing movement model and two new body geometry models (one for a blood-fed mosquito and another for an unfed mosquito) (Movies 5 and 6). The wing model was based on cubic smoothing spline fits of the outline of 20 female mosquito wings. The wing movement model was made by manually tracking three consecutive wingbeats of both a blood-fed and an unfed mosquito in free flight (Fontaine et al., 2009). The automatic tracker performance was poor when tracking initial wing movements at the start of the take-off, and therefore we used a manual tracker to determine wing positions during this phase of the take-off (Fontaine et al., 2009).

At each consecutive video frame, both trackers provided us with a time stamp t , a body position ($\mathbf{X}=\{x,y,z\}$) and orientation (expressed by a body quaternion \mathbf{q}_b) in the global reference frame, and the angular orientations of the wings within the body reference frame (expressed as quaternions \mathbf{q}_L and \mathbf{q}_R for the left and right wing, respectively) (Fontaine et al., 2009). The z -axis of the global reference coordinate system was oriented vertically upwards, and the origin of the coordinate system was set at the body position at the start of the maneuver ($\mathbf{X}_{\text{start}}=\{0,0,0\}$), defined as the moment that the mosquito started moving its wings. Maneuvers were aligned in time such that lift-off occurred at $t=0$ s, whereby lift-off was defined as the point in time when the last leg left the platform. We then separated each take-off maneuver into a push-off phase ($t<0$ s) and a flight phase ($t>0$ s).

The body positions throughout each take-off sequence were post-processed using a linear Kalman filter (Muijres et al., 2014), which provided us with the time series of body position $\mathbf{X}(t)$, velocity $\mathbf{U}(t)$ and acceleration vectors $\mathbf{a}(t)$. From the body positions, we determined the body-length-normalized displacements at lift-off,

$X_{\text{lift-off}}/l_{\text{body}}$, whereby l_{body} is body length. From the velocity vectors, we determined flight speed $U(t)$, ascent angle $\gamma(t)$ and flight heading through time (Fig. 3C). From the body accelerations and the gravitational acceleration vector ($\mathbf{g}=\{0,0,g\}$), we determined the weight-normalized external forces on the animal as:

$$\mathbf{F}(t)/mg = (\mathbf{a} + \mathbf{g})/|g|. \quad (4)$$

By multiplying \mathbf{F}/mg with the mass ratio of the animal, we determined the unfed-weight normalized external force on the animal as:

$$\mathbf{F}/mg_{\text{unfed}} = R_m \cdot \mathbf{F}/mg. \quad (5)$$

The first parameter (\mathbf{F}/mg) indicates the amount of g -force that an animal produced throughout the take-off, whereas the second parameter ($\mathbf{F}/mg_{\text{unfed}}$) shows how forces varied with both body acceleration and the weight increase as a result of blood feeding. Body orientations (\mathbf{q}_b) were post-processed using an extended Kalman filter (Muijres et al., 2014), and were converted into body

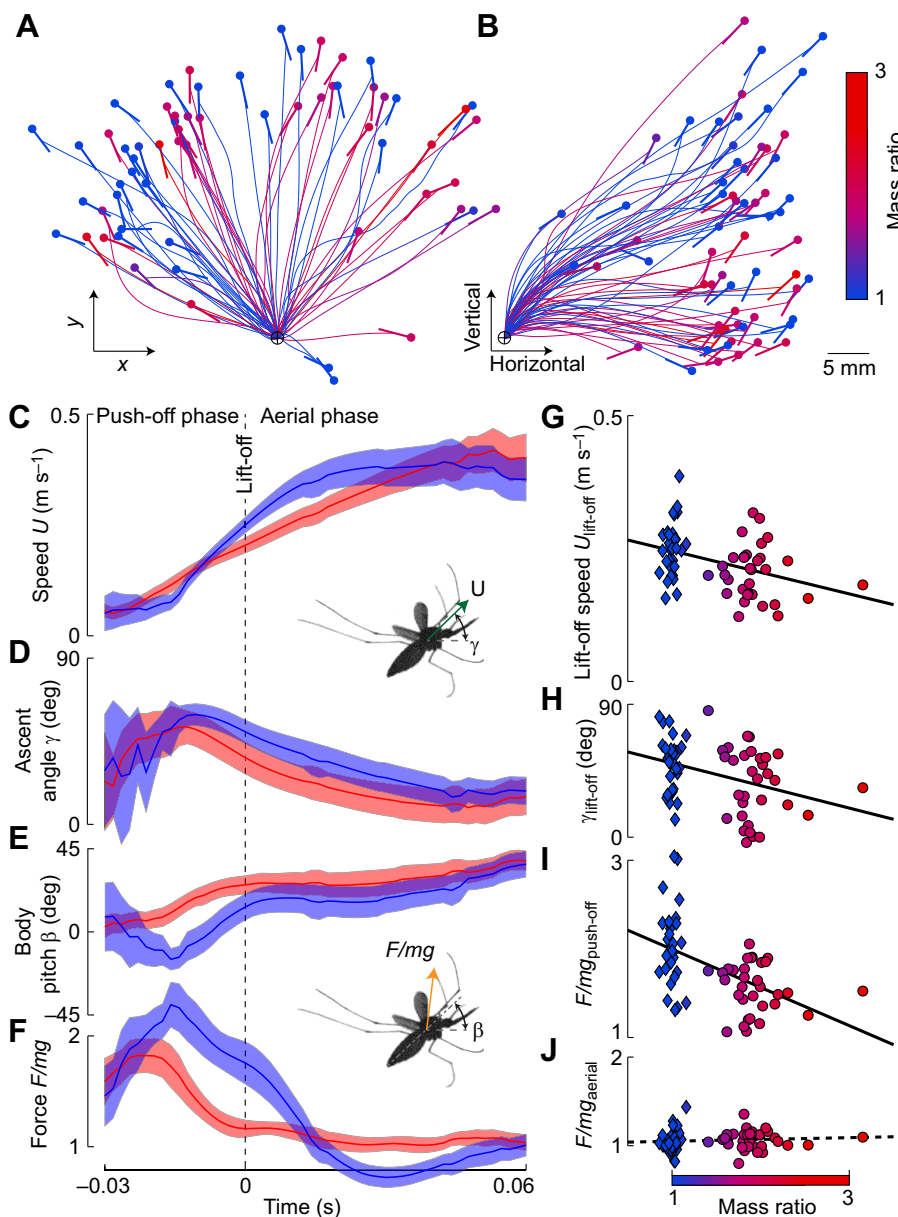


Fig. 3. Take-off dynamics of blood-fed (red) and unfed (blue) mosquitoes. (A,B) Flight path (thin lines) and orientation of the longitudinal body axis (lollypops, whereby the circles indicate head position, and stick length represents body length), viewed from above (A) and the side (B), whereby horizontal displacement is defined as the vector sum of $\{x,y\}$. (C–F) Temporal dynamics of flight speed (C), ascent angle (D), body pitch (E) and normalized force (F). All trajectories are aligned such that lift-off (absence of tarsal contact) occurs at $t=0$ s. Traces indicate mean and confidence interval at each video frame ($13,500 \text{ frames s}^{-1}$). (G–J) Effect of body mass on speed and ascent angle at lift-off (G,H), and average normalized force during the push-off phase and aerial phase (I and J, respectively). In A, B and G–J, data for each mosquito are color-coded by mass ratio R_m , as indicated by the color bar in B.

pitch angle β and body orientation angle ψ throughout the take-off (Fig. 3E).

The quaternions of wing orientation (\mathbf{q}_L and \mathbf{q}_R) were Kalman filtered and converted into the three Euler angles within the stroke-plane reference frame (Fig. 1B) (Muijres et al., 2014): stroke angle $\phi(t)$, deviation angle $\theta(t)$ and wing rotation angle $\eta(t)$. The stroke-plane reference frame was fixed relative to the body at a 47.5 deg pitch-down angle with respect to the longitudinal body axis. Like fruit flies (Muijres et al., 2014), steadily flying unfed mosquitoes have a body pitch angle of approximately 47.5 deg, and thus for steady flight the stroke plane defined here is oriented nearly horizontally. Note that blood-fed mosquitoes and unfed mosquitoes during take-off maneuvers can operate at very different body angles (Fig. 3E).

Based on the stroke angle, we separated each flight sequence into separate wingbeats, whereby the start of each wingbeat is defined as the moment at which the stroke angle is maximal (the wing is positioned at its dorsal extreme, Fig. 1B). Each wingbeat was then divided into a downstroke and an upstroke, whereby the former is defined as a wing movement from the dorsal to the ventral side of the body, and the latter proceeds in the opposite direction. Note that during steady flight, when the stroke plane is oriented horizontally, these are actually forward and backward wing movements, but to remain consistent with existing literature, we termed them downstroke and upstroke, respectively.

For each wingbeat, we determined the flapping frequency $f=1/\Delta t$, where Δt is the time window between the start of two consecutive wingbeats. Stroke amplitude was defined as $A_{\text{stroke}}=\phi_{\text{max}}-\phi_{\text{min}}$, and wing rotation amplitude was defined as $A_{\text{rotation}}=\eta_{\text{max}}-\eta_{\text{min}}$. To study the effect of changes in body pitch on the wingbeat kinematics, we defined the stroke-plane pitch angle adjustment as the difference in pitch angle between the real stroke plane and the body-fixed stroke-plane reference frame (Fig. 1B). The real stroke plane is the curved surface that follows the wing tip path throughout the wingbeat (Fig. 4K). Thus, the adjustment of the stroke-plane pitch angle is calculated by:

$$\sigma = \tan^{-1}(A_{\text{deviation}}/A_{\text{stroke}}), \quad (6)$$

where $A_{\text{deviation}}$ is the deviation angle amplitude, defined as the difference between the deviation angle at the start of the downstroke and at the start of the upstroke (Fig. 4B,K).

Modeling aerodynamic force production based on wingbeat kinematics

Based on the measured wing morphology and wingbeat kinematics, we modeled the aerodynamics of the take-off maneuvers using a computational quasi-steady blade-element aerodynamic model that simulates both translational and rotational aerodynamic forces generated by flapping insect wings (Muijres et al., 2014; Sane and Dickinson, 2002). For this, we divided the mosquito wing into 20 spanwise segments, and each wingbeat into 200 time steps. For each combination of wing segment and time step, we calculated the angle of attack, translational velocity and rotational velocity (i.e. the rotational angle flux). Based on the chord length, wing velocity and angle of attack of each wing section and time segment, we calculated its lift and drag production using the translational force model; based on chord length, the translational velocity and the angular velocity about the wing rotation axis, we determined rotational lift production.

For the model, we used the functions of lift and drag coefficients versus angle of attack [$C_L(\alpha)$ and $C_D(\alpha)$, respectively] and the

rotational lift coefficients ($C_{\text{rot}}=1.55$) determined using a robotic insect wing model, as mosquitoes operate at a Reynolds number similar to that used in the robot (Sane and Dickinson, 2002). This quasi-steady model captures aerodynamic force production remarkably well in flapping fruit fly wings (Dickinson and Muijres, 2016; Sane and Dickinson, 2002), but it does not simulate unsteady aerodynamic effects, such as wake capture, added mass or the trailing-edge vortex lift that was recently identified as an important lift generator in flying mosquitoes (Bomphrey et al., 2017). This recent study on the aerodynamics of male *Culex* mosquitoes also developed a quasi-steady aerodynamic model (Bomphrey et al., 2017). This model produced different estimates for $C_L(\alpha)$ and $C_D(\alpha)$, which might be because it is based on computational fluid dynamics simulations rather than robotic model experiments, or (more likely) because it was based on simulations of high-aspect ratio mosquito wings.

Analyzing time-derived kinematics and force dynamics throughout the take-off

During the push-off phase of the take-off maneuver ($t < 0$ s), mosquitoes can combine leg-derived push-off forces with wing-derived aerodynamic forces, whereas during the flight phase of the maneuver ($t > 0$ s), wingbeat-averaged external forces consist only of aerodynamic forces, primarily produced by the beating wings. To estimate the relative contribution of these forces, we analyzed the time-derived kinematics and force dynamics throughout the take-off maneuver in detail (Fig. 5). Because this required labor-intensive manual tracking, we performed this analysis on a random subset of eight blood-fed and eight unfed mosquitoes. For each mosquito, we estimated aerodynamic forces throughout the take-off (F_{aero}) using our aerodynamic model, and total forces were calculated from body accelerations (F_{total} , Eqns 4–5). During the flight phase of the maneuver ($t > 0$ s), total forces and aerodynamic forces should be equal, whereas during the push-off phase ($t < 0$ s), the difference between total force and aerodynamic force should be equal to the leg-induced forces ($F_{\text{leg}}=F_{\text{total}}-F_{\text{aero}}$). To compare aerodynamic forces with total forces, we calculated the wingbeat-average aerodynamic forces using a low-pass Butterworth filter with a cut-off frequency half that of the mean wingbeat frequency of our mosquitoes. For each tested mosquito, we then calculated the ratio between the mean aerodynamic forces and leg force throughout the push-off phase as $F_{\text{aero}}/F_{\text{leg}}$.

Statistical aerodynamic force control model for blood-load-carrying mosquitoes

We studied how mosquitoes change their wing movement pattern and aerodynamic force production to carry a blood load. For this, we focused on the flight phase of the take-off because wingbeat-averaged aerodynamic forces in this case should equal forces estimated from body accelerations. We used two complementary approaches.

First, for each wingbeat-tracked mosquito, we determined the average stroke amplitude, wing rotation amplitude, stroke-plane pitch adjustment angle and wingbeat frequency throughout the flight maneuver. And we correlated these parameters with the average unfed-weight normalized aerodynamic force produced during the flight phase (F/mg_{unfed} ; Eqns 4, 5).

Second, to more systematically determine how the changes in wingbeat kinematics affect aerodynamic force production, we used an analysis method similar to that used to study evasive dynamics of free-flying fruit flies (Muijres et al., 2014). We first parsed the complete dataset of free-flight tracked wingbeats into three subsets: wingbeats of blood-fed mosquitoes, wingbeats of unfed

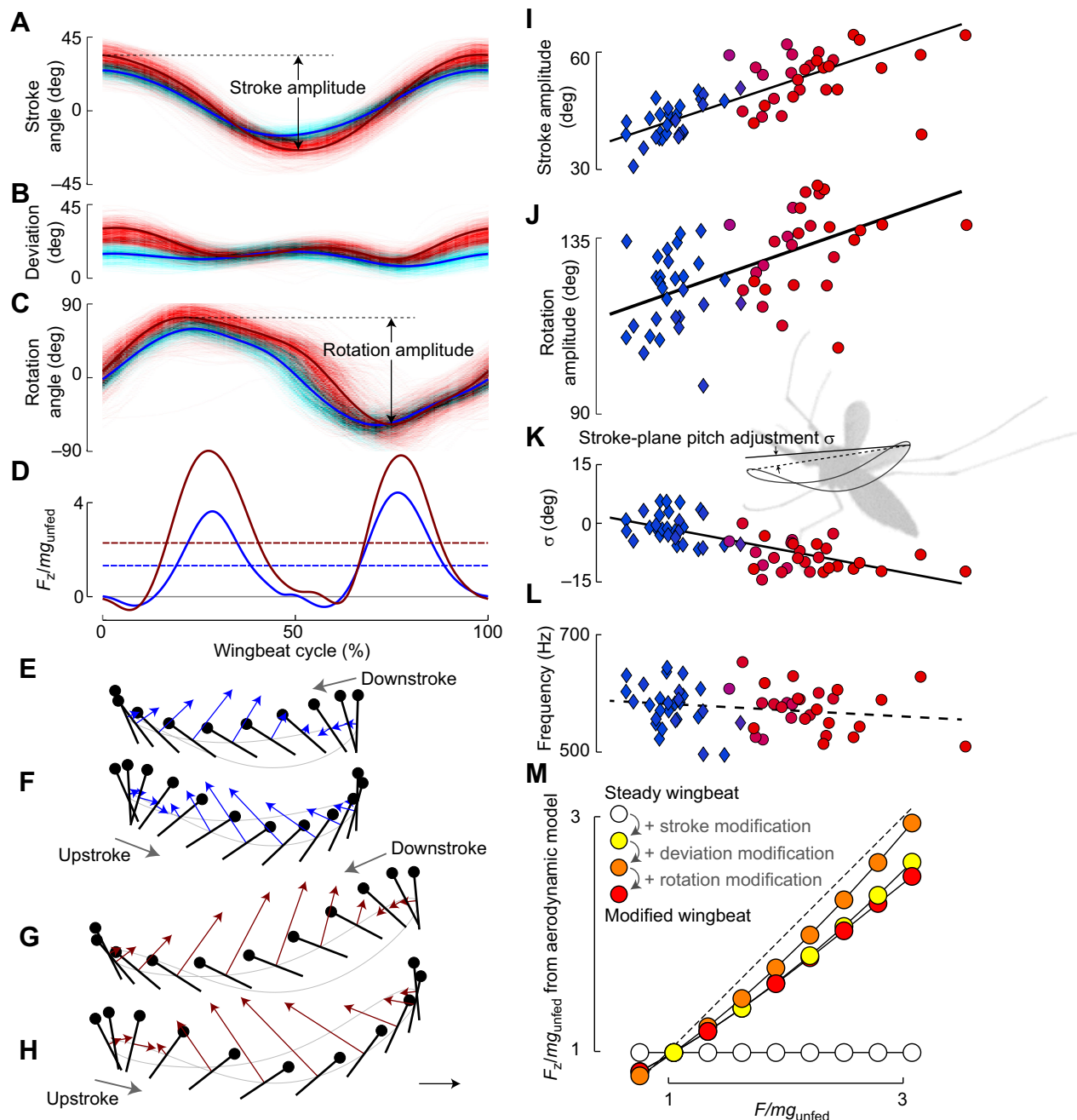


Fig. 4. Wingbeat kinematics and aerodynamics of unfed (blue) and blood-fed (red) mosquitoes during the aerial phase of the take-off. (A–D) Wingbeat kinematics (A–C) and aerodynamic forces (D) throughout the wingbeat cycle. (A–C) The red channel shows a heat map of all free flight wingbeats for blood-fed mosquitoes, and the cyan channel indicates a heat map of all wingbeats for unfed steadily flying mosquitoes. The blue traces show Fourier series fits on all steady wingbeats for unfed individuals, whereas the dark red trace indicates the statistical model reconstruction (Eqn 9) for the average blood-fed mosquito with $F/mg_{unfed}=2.21$. (D) Total vertical forces calculated using our aerodynamic model for the average unfed (blue) and blood-fed (red) mosquito. (E–H) Wingtip path (lollypops) and force vector (colored) representation of data in A–D. Downstroke and upstroke are separated for legibility. (I–L) Effect of aerodynamic force enhancement (expressed by F/mg_{unfed}) on stroke amplitude (I), rotation angle amplitude (J), stroke-plane pitch adjustment (K) and wingbeat frequency (L); each data point represents a single mosquito, color-coded with its mass ratio (see color bar in Fig. 2B). (M) Wingbeat-averaged vertical force production for a series of steadily flying hypothetical mosquitoes with a range of blood loads (expressed by F_z/mg_{unfed}), and whereby we systematically replaced steady flight wingbeat parameters with that of their modified kinematics (Eqn 9).

mosquitoes flying steadily and wingbeats of unfed mosquitoes when maneuvering. Wingbeats were characterized as steady when wingbeat-averaged body accelerations were less than $0.25 g$, where g is gravitational acceleration (Muijres et al., 2014).

By fitting a Fourier series through the subset of all unfed steady-flight wingbeats, we determined the average wingbeat kinematics

of a steadily flying unfed malaria mosquitoes. The Fourier series were fitted using a Levenberg–Marquardt algorithm, and are defined as:

$$k_{\text{steady}}(\tau) = a_0 + \sum_{n=1}^N a_n \cos(2\pi n\tau) + b_n \sin(2\pi n\tau), \quad (7)$$

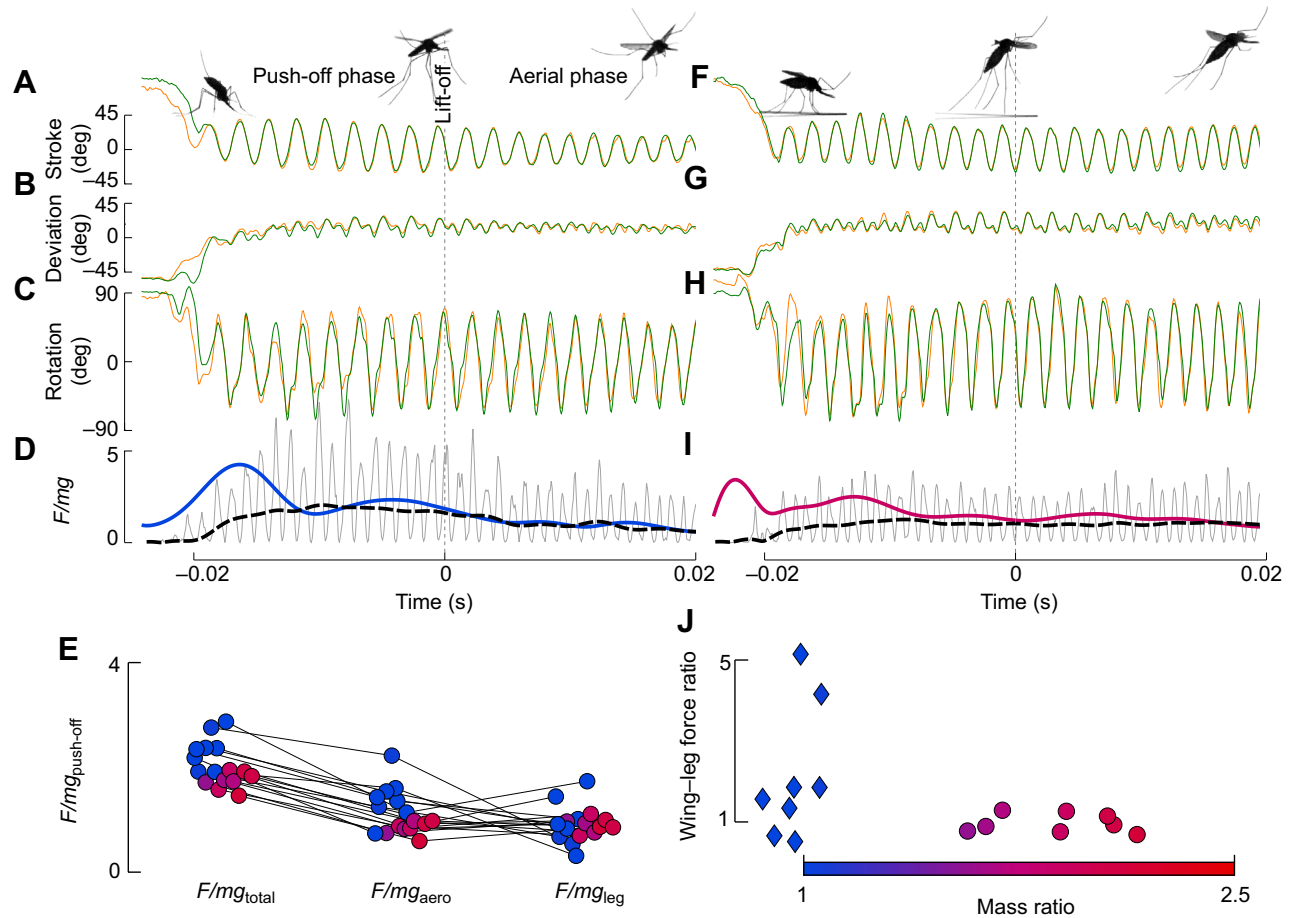


Fig. 5. Leg forces and wing-derived aerodynamic forces during the push-off phase of the take-off. (A–D) Wingbeat kinematics (A–C, left wing in green, and right in orange), and weight-normalized forces (D) during the take-off of an unfed mosquito. The equivalent data for a blood-fed mosquito are shown in F–I. A and F also show lateral views of the mosquitoes at the start of the maneuver, at lift-off ($t=0$ s) and at the end of the sequence. (D, I) Total force based on body acceleration (in color) and aerodynamic forces calculated using the quasi-steady model. The gray trace indicates aerodynamic force variations through each wingbeat, and the dashed black trace represents wingbeat-averaged forces. (E, J) Mean forces during the push-off phase ($t < 0$ s) for all measured mosquitoes: (E) mean total force, aerodynamic force and leg-derived force, and (J) the ratio between aerodynamic and leg-derived forces versus mass ratio.

where k_{steady} is the steady-flight wing kinematics variable (ϕ_{steady} , θ_{steady} or η_{steady}), τ is normalized time ($\tau = t/\tau$), and a_n and b_n are the coefficients of the n th order Fourier series. For the stroke angle, we fitted a fourth order Fourier series, whereas for the deviation and rotation angles we fitted a sixth order series because of higher harmonics in their temporal dynamics.

Based on the dataset of wingbeats tracked from blood-fed mosquitoes, we determined how mosquitoes adjust their wing movement in order to carry the extra load of a blood meal. For this, we used a linear model that correlated changes in wingbeat kinematics (with respect to the above-derived steady kinematics, k_{steady}) with changes in force production (relative to steady flight force production, $F/mg_{unfed,steady}$). Thus, for every kinematics parameter $k = \phi, \theta$ or η of wingbeat number i , we calculated the wing kinematic modification:

$$\text{mod}_{k,i} = (k_i - k_{steady}) / (F/mg_{unfed,i} - F/mg_{unfed,steady}). \quad (8)$$

We determined the average modification parameters (MOD_k) for each kinematics variable k by fitting sixth order Fourier series through the temporal distributions of the complete $\text{mod}_{k,i}$ dataset (Eqn 7). From the resulting set of modification parameters (MOD_ϕ , MOD_θ , MOD_η), we then could reproduce the set of wingbeat kinematics that a hypothetical mosquito would generate to carry its

body weight plus a blood load with a combined normalized weight of F/mg_{unfed} , from:

$$k = k_{steady} + \text{MOD}_k \cdot (F/mg_{unfed} - F/mg_{unfed,steady}). \quad (9)$$

Using this model, we derived wing kinematics of nine hypothetical mosquitoes carrying a load of -25% to 175% of the average blood load of all fed mosquitoes (with a step size of 25%). Note that a mosquito with a 0% load equals the average unfed mosquito, and at 100% the hypothetical mosquito has a blood load equal to that of the average blood-fed mosquito, and thus this distribution of body masses encompasses the full mass range of our experimental mosquitoes. Based on the wing kinematics of each hypothetical mosquito, we estimated aerodynamic forces using our aerodynamic model, and we also compared the wingbeat-averaged values with the required forces based on body mass and blood load.

To determine the effect of the various wingbeat kinematics parameters on aerodynamic force production, we performed a second set of aerodynamic model simulations. For each hypothetical mosquito, we incrementally replaced the steady-flight wingbeat kinematics with its modified kinematics in the following order: first, we ran each case with the full steady kinematics k_{steady} ; second, we allowed each hypothetical mosquito to adjust only the stroke angle; third, deviation angle was also

varied; and finally, variations in wing rotation angle were added, resulting in completely modified kinematics (changes in wingbeat frequency were not modeled because these did not change significantly with blood load). For each combination of kinematics and blood load, we calculated the wingbeat-average aerodynamic forces using the quasi-steady aerodynamic model.

Statistical analysis of flight dynamics throughout the take-off maneuvers

We performed four sets of statistical tests (Tables S1–S4). First, we tested whether take-off dynamics differed significantly between mosquitoes that performed either a voluntary take-off or a take-off triggered by substrate vibrations (Table S1). Because these did not differ significantly from one another (Table S1), we combined voluntary and triggered individuals in all subsequent analyses. Second, we tested the effect of feeding condition (unfed versus blood-fed) on kinematics and force production throughout the take-off (Table S2), and third, on the wingbeat kinematics during the aerial phase of the take-off (Table S3). For the fourth test, we compared the relative contribution of leg-derived push-off forces and wing-derived aerodynamic forces to total force production during the push-off phase of the take-off (Table S4). For all statistical tests, we used a Shapiro–Wilk test to determine whether the different groups were normally distributed. Because the majority of groups were not normally distributed, we used the non-parametric Mann–Whitney *U*-test for all consecutive statistical tests. We report results both as means±s.d. and as medians (first quartile – third quartile) (Tables S1–S4).

Leg and flight muscle morphology in malaria mosquitoes

Using our mosquitoes, we were unable to trigger those escape responses described in fruit flies, for which 100% of the push-off forces are produced by the middle pair of legs (Card and Dickinson, 2008b). Fruit flies perform such escape take-offs in response to visual looming stimuli, as mediated by the giant axon that triggers the large TDT muscle between the middle leg and the top of the thorax (Card and Dickinson, 2008b). Tsetse flies have been shown to have lost the giant axon and TDT muscle, and therefore are not thought to be able to perform this dedicated leg-based take-off (King, 1983).

We made μ CT scans of the thorax of a female malaria mosquito using the Tomographic Microscopy and Coherent Radiology beamline (TOMCAT) of the Swiss Light Source at the Paul Scherrer Institut, Switzerland (Stampanoni et al., 2010), from which we reconstructed the 3D morphology of the leg and flight muscles. To prepare the specimen, we used a staining method developed for increasing contrast of non-mineralized tissues (Metscher, 2009). For this, we first fixed the specimen with Bouin solution for 1 day, followed by several rinsing steps with decreasing ethanol concentrations (70%–50%–30%). After an additional series of rinsing steps with demineralized water with 0.05% Tween® 20 (VWR Int. BV), the specimen was stained with a 10% IKI (Lugol's iodine) solution. The thorax was preserved in this IKI solution during transportation to the Swiss Light Source. Using the TOMCAT beamline, we scanned the thorax at 18 keV, with an exposure time of 10 μ s at 10 times magnification. The resulting stack of image slices was further processed using the software program for medical image processing and visualization MeVisLab (MeVis Medical Solutions AG, Bremen, Germany), allowing us to individually segment different muscles within the thorax of the mosquito (Figs 1D, 6). We identified the indirect flight power muscles, the dorso-ventral muscles (DVMs) and the dorso-

longitudinal muscles (DLMs), and the extracoxal depressor muscles of the trochanter of the front, middle and hind leg (EDT1, EDT2 and EDT3, respectively). Three-dimensional reconstructions of these muscles were visualized using the medical imaging programs MeVisLab and Meshlab (Cignoni et al., 2008). Note that the EDT2 muscle is homologous to the TDT found in several fly species and used to power escape take-offs (Card and Dickinson, 2008a,b).

RESULTS

Maneuver dynamics throughout the take-off

In total, we filmed and analyzed the take-off dynamics of 32 blood-fed and 31 unfed female mosquitoes performing either voluntary (17 blood-fed and 15 unfed individuals) or escape (15 blood-fed and 16 unfed individuals) take-offs from the experimental platform (Fig. 3A,B, Movie 7; see database S1 in Muijres et al., 2017). Based on morphological measurements, we estimated that the blood-fed mosquitoes averaged twice the mass of unfed mosquitoes (ratio of the total mass of blood-fed animals to the mass of unfed animals, $R_m = m_{\text{bloodfed}}/m_{\text{unfed}} = 1.93 \pm 0.32$, $n=32$, where $m_{\text{unfed}} = 1.23 \pm 0.08$ mg, $n=31$; Fig. 1C). Each take-off consisted of a push-off phase and an aerial phase, separated by lift-off ($t=0$ s) when the last leg leaves the platform (Fig. 3A–F). This occurred in 21%, 57% and 22% of the cases for the front, middle and hind legs, respectively. During the push-off, mosquitoes combined aerodynamic forces produced by the beating wings with push-off forces from the legs to boost body accelerations (Fig. 2, Movies 1–4), yielding the highest forces, accelerations and ascent angles (Fig. 3C–F). During the aerial phase, the animal necessarily used only wing-derived aerodynamic forces, which were lower and more constant through time (Fig. 3F).

None of the calculated take-off parameters differed significantly between voluntary and escape take-offs (Table S1); therefore, we combined the voluntary and triggered individuals in all subsequent analyses. In contrast, most of the take-off parameters did differ between the take-offs of blood-fed and unfed mosquitoes (Table S2): during the push-off phase, unfed mosquitoes attained higher accelerations, speeds and ascent angles than did those carrying the additional load of a blood meal (Fig. 3C,D,G,H). Although absolute forces produced during the push-off phase were higher for the blood-fed mosquitoes, the ratio of peak force produced relative to body weight was 2.03 for unfed mosquitoes, but only 1.56 for blood-fed animals (Fig. 3F,I, Table S2). In contrast, during the aerial phase, the ratio of mean aerodynamic force to body weight did not differ between blood-fed and unfed animals (Fig. 3J, Table S2). Thus, malaria mosquitoes enhanced aerodynamic forces proportionally to their weight increase from blood feeding, suggesting that aerodynamic force production was not limited within the range of tested blood loads. During the push-off phase, body pitch angles of blood-fed mosquitoes carrying this extra abdominal load were higher than those of unfed individuals (Fig. 3E, Table S2).

Aerodynamic force control for carrying blood loads

Our analysis of wingbeat kinematics during the aerial phase (Fig. 4) shows that, similar to *Culex* mosquitoes (Bomphrey et al., 2017), steadily flying unfed malaria mosquitoes operate at exceptionally low wingbeat amplitudes ($A_{\text{stroke}} = 42$ deg) and high wingbeat frequencies ($f = 579$ Hz; Fig. 4I,L, Table S3). To carry a blood load, blood-fed mosquitoes adjust their wing movement pattern (Fig. 4A–C) by increasing their stroke amplitude, rotation amplitude and stroke-plane pitch adjustment angle (Fig. 4I–K, respectively). But

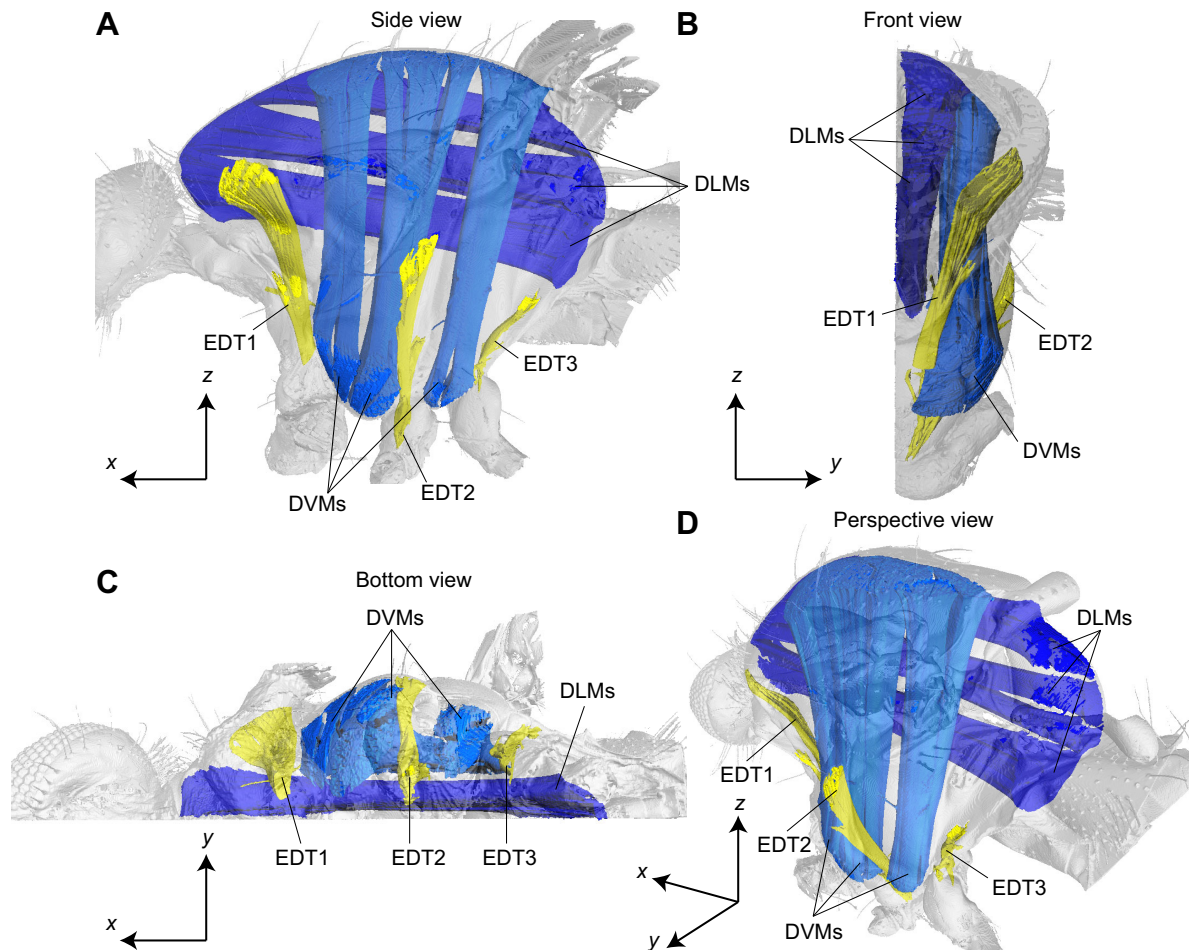


Fig. 6. Three-dimensional μ CT reconstruction of the muscular system within the left half of the thorax of a female malaria mosquito. The indirect flight power muscles (blue) consist of the dorso-ventral and dorso-longitudinal muscles (DVMs and DLMs, respectively). The leg muscles that mostly power push-off (yellow) are the extracoxal depressor muscles of the trochanter of the front, middle and hind leg (EDT1, EDT2 and EDT3, respectively). Surrounding material that was stained but did not belong to the segmented muscles was visualized in transparent gray.

strikingly, wingbeat frequency did not change significantly with force production (Fig. 4L, Table S3).

In total, we tracked 1620 wingbeats during the areal phase of the 63 take-off maneuvers, based on which we tested how changes in wingbeat kinematics affect aerodynamic force production (Fig. 4A–C; see database S2 in Muijres et al., 2017). The pooled dataset of 1620 wingbeats consisted of 264 wingbeats of steadily flying unfed mosquitoes, 840 wingbeats of maneuvering unfed mosquitoes and 516 wingbeats of blood-fed mosquitoes. By fitting Fourier series onto the 264 wingbeats of steadily flying unfed mosquitoes (Eqn 7), we determined the mean wingbeat kinematics of steady-flying unfed malaria mosquitoes (Fig. 4A–C; see database S2 in Muijres et al., 2017). The corresponding average wingbeat frequency of the steadily flying unfed mosquitoes was $f_{\text{steady}}=577\pm 41$ Hz ($n=264$). Based on the body kinematics, we estimated the concomitant aerodynamic force production at $F/mg_{\text{unfed,steady}}=1.05\pm 0.11$, a flight speed of $U_{\text{steady}}=0.23\pm 10$ m s⁻¹ and a body pitch angle of $\beta_{\text{steady}}=48\pm 9$ deg.

By applying our statistical model for aerodynamic force control (Eqn 8) to the 516 wingbeats of the blood-fed mosquitoes, we expressed how mosquitoes adjust their wingbeat kinematics for load-carrying, which resulted in a set of three Fourier series (for stroke angle, pitch angle and wing rotation angle, see database S2 in Muijres et al., 2017). The associated wingbeat-average force production for the 516 wingbeats of the blood-fed mosquitoes

was estimated at $F/mg_{\text{unfed}}=2.21$ (Eqns 4 and 5). We reconstructed the wingbeat kinematics for a mosquito that would produce this normalized force (Eqn 9 with $F/mg_{\text{unfed}}=2.21$) and compared this with the 516 original wingbeats (Fig. 4A–C). The reconstructed kinematics for the average blood-fed mosquito (dark red traces in Fig. 4A–C) overlay well onto the traces of all tracked wingbeats (red heat map in Fig. 4A–C), suggesting that the linear statistical model for force enhancement accurately captures the dynamics found in real blood-fed mosquitoes.

To study how aerodynamic forces differed between steady flight of unfed mosquitoes and flight of the average blood-fed mosquito, we replayed the wingbeat kinematics for both cases (blue and red traces in Fig. 4A–C, respectively) in our aerodynamic model and determined the temporal dynamics of the aerodynamic forces (blue and red traces in Fig. 4D–H, respectively). We then compared the wingbeat-average aerodynamic force F_{aero} with the force prediction from body acceleration and weight (F_{total} , Eqns 4–5) by calculating the ratio $F_{\text{aero}}/F_{\text{total}}$. For the unfed mosquito case, $F_{\text{aero}}/F_{\text{total}}=0.97$, while for the average blood-fed mosquito, $F_{\text{aero}}/F_{\text{total}}=0.83$. Thus, for the unfed mosquitoes, the quasi-steady model captures the required aerodynamic forces remarkably well, whereas for the average blood-fed mosquito, aerodynamic forces were underestimated by 17%. Our systematic study whereby we reconstructed kinematic patterns for the nine hypothetical

mosquitoes with varying blood loads (Eqn 9) and then modeled their aerodynamic force production confirms this dynamics (Fig. 4M): for an unfed mosquito the quasi-steady model predicts aerodynamic forces rather well, but with increasing body weight the model increasingly underestimates total force production.

The set of nine hypothetical mosquitoes was also used to test how adjustments of the different kinematics parameters with variations in blood load affect aerodynamic force production (Fig. 4M). The increased force production for carrying a blood load was almost fully explained by the variations in stroke angle kinematics, whereby an increase in stroke amplitude results in an enhancement of the aerodynamic force. The changes in deviation angle also slightly increased force production, but this was fully negated by concomitant changes in wing rotation angle.

Leg-based and wing-derived forces throughout the push-off

For a random subset of eight blood-fed and eight unfed mosquitoes, we tracked the transient wingbeat kinematics throughout the complete take-off, including the push-off phase and the aerial phase (Fig. 5A–C,F–H). We then calculated total external force production based on body accelerations (Eqns 4–5), and wing-derived aerodynamic forces using our aerodynamic model (Fig. 5D,I).

To determine relative contributions of legs and wings to force production during the push-off phase, we compared instantaneous total external force (due to both legs and wings, F/mg_{total}) with the wingbeat-average aerodynamic forces (F/mg_{aero} , Fig. 5E). During the aerial phase, total force and aerodynamic force were not significantly different (Table S4), suggesting that it is valid to estimate leg forces during the push-off phase as the difference between total forces and the aerodynamic forces (F/mg_{leg} , Fig. 5E). From these results, we then calculated the ratio between aerodynamic force and leg forces ($F_{\text{aero}}/F_{\text{leg}}$, Fig. 5J). These did not differ significantly between unfed and blood-fed mosquitoes (Table S4), suggesting that blood-fed mosquitoes do not change their take-off behavior relative to unfed mosquitoes, and that they increased force production proportionally with their weight increase after blood-feeding. Combining $F_{\text{aero}}/F_{\text{leg}}$ from blood-fed and unfed mosquitoes shows that during the push-off phase, mosquitoes produced aerodynamic forces that were, on average, ~50% higher than the leg-produced forces ($F_{\text{aero}}/F_{\text{leg}}=1.55\pm 1.29$, $n=16$; Table S4).

The effect of push-off force production on tactile detection by the host

To avoid detection by a mammalian blood-host, an escaping blood-fed mosquito should reduce ground reaction forces to at least less than 0.07 mN (Li et al., 2011). Based on the momentum equation, the lift-off speed of a flying animal depends on the push-off force and push-off duration as follows:

$$U_{\text{lift-off}} = F/mg_{\text{push-off}} \cdot \Delta t_{\text{push-off}} \cdot g. \quad (10)$$

Therefore, a reduction in force production directly leads to a decrease in take-off speed. Based on our take-off dynamics data, we tested how mosquitoes negate this apparent trade-off between stealth and speed during take-off. Take-off speed also depends on the duration of the push-off phase, $\Delta t_{\text{push-off}}$ (see Eqn. 10), and thus, by extending the push-off phase, a mosquito can reduce push-off force without affecting take-off speed.

Mosquitoes have relatively long legs (the average length of the front, middle and hind legs of our mosquitoes equaled 109%, 138% and 169% of their body length, respectively), which they almost fully extending throughout the push-off phase (Fig. 2, Movies 1–4).

As a result, our mosquitoes traveled, on average, 88% of their body length away from the substratum while continuing to push off with their legs ($X_{\text{lift-off}}/l_{\text{body}}=0.88\pm 0.37$, $n=63$). The resulting push-off duration was $\Delta t_{\text{push-off}}=26.3\pm 11.5$ ms, and their lift-off speed was $U_{\text{lift-off}}=0.23\pm 0.05$ m s⁻¹.

Exchanging leg-derived push-off forces for wing-derived aerodynamic forces might further reduce peak force production on the host's skin. Wing-derived aerodynamic forces produced by a flying animal generate forces on the substrate in the form of pressure waves (Anderson, 1991; Lentink et al., 2015). According to actuator disk theory, these forces are distributed across a circular area with a radius comparable to the animal's wing span, or a sub-section of this disk for low-amplitude flapping wings (Ellington, 1984). In both cases, the aerodynamic pressure waves will be distributed across several mechanosensors. In contrast, point-load forces produced by a mosquito leg can potentially trigger a single hair sensor, and thus leg forces have a much higher likelihood to be detected. We estimated peak forces during the push-off phase in our blood-fed mosquitoes by:

$$F_{\text{push-off,max}} = F/mg_{\text{push-off,max}} \cdot R_m \cdot m_{\text{unfed}} \cdot g. \quad (11)$$

With $F/mg_{\text{push-off,max}}=2.01$ and $R_m=1.93$ for the average blood-fed mosquito, this results in a peak push-off force of $F_{\text{push-off,max}}=0.05$ mN. The leg-based force component of this peak force is estimated by:

$$F_{\text{leg,max}} = F_{\text{push-off,max}} \cdot F_{\text{leg}}/F_{\text{total}}, \quad (12)$$

where the ratio of leg and total forces is $F_{\text{leg}}/F_{\text{total}}=0.39$, as determined in the analysis of the force dynamics during the push-off phase (Fig. 5). This leads to a peak leg push-off force for the average blood-fed mosquito of $F_{\text{leg,max}}=0.02$ mN. Both the total peak push-off force and the leg-based peak force are below the 0.07 mN threshold for mechanosensory hairs of mammals (Li et al., 2011), suggesting that mammals cannot detect push-off forces of blood-fed malaria mosquitoes.

Leg and wing muscle morphology of malaria mosquitoes

Push-off forces and aerodynamic forces required for take-off are generated by the leg muscles and the indirect flight power muscles, respectively. Based on the μ CT scans, we reconstructed the most important muscles of these systems (Figs 1D, 6, Movie 8; see database S3 in Muijres et al., 2017). We identified flight power muscles (DVMs and DLMS, respectively), and the leg muscles that mostly power push-off: EDT1, EDT2 and EDT.

The EDT2 muscle is homologous to the TDT found in several fly species, and these flies use to power escape take-offs (Card and Dickinson, 2008a,b). In flies, this TDT muscle is similar in size and orientation to the DVMs. But, as in tsetse flies (King, 1983), the EDT2 muscle in the female malaria mosquito is much smaller than the DVMs, and is not attached to the tergal side of the thorax (Fig. 6, Movie 8). Thus, as in tsetse flies, mosquitoes lack a TDT muscle specialized for performing take-off escape maneuvers.

DISCUSSION

Kinematics and aerodynamics of blood-load carrying in malaria mosquitoes

Our blood-fed mosquitoes were carrying a blood load roughly equal to their body weight, and were still capable of performing rapid take-off maneuvers (Fig. 3, Movies 3, 4). The adjustments to wing and leg kinematics that enable mosquitoes to carry this extra weight

are surprisingly simple (Fig. 4). To boost aerodynamic force production for carrying a blood meal, mosquitoes relied almost completely on an increase in wing stroke amplitude (Fig. 4A,I,M), whereas wingbeat frequency was not altered (Fig. 4L). Mosquitoes also adjusted both the wing deviation angle and rotation angle (Fig. 4B,C,J,K), but these changes had only small effects on force production (Fig. 4M). Instead, changes in deviation and rotation angles were associated with changes in body pitch: mosquitoes with abdominal blood loads were oriented more vertically than unfed animals (Fig. 3E), and thus a concomitant nose-down rotation of the stroke plane was required to continue alignment of the aerodynamic lift vector with the vertical body weight vector (Fig. 4K).

For a series of hypothetical mosquitoes with a range of blood loads, we compared wingbeat-averaged aerodynamic forces with their body weight, showing that aerodynamic forces were similar to the forces required for weight support (Fig. 4M). However, with increasing blood loads, the difference between required force and the aerodynamically modeled force increasingly differed (Fig. 4M). This is most likely because of the limitations of our quasi-steady aerodynamic model which did not include several unsteady aerodynamic mechanisms, such as wake capture and added mass (Dickinson and Muijres, 2016). These unsteady aerodynamic mechanisms might thus become increasingly more important with greater force production; in particular, trailing-edge vortex lift, which was recently described in flying mosquitoes, might play an important role here (Bomphrey et al., 2017). Future research into the detailed aerodynamics of mosquito flight is required to answer this question.

The hovering kinematics of our malaria mosquitoes are similar to those of *Culex* mosquitoes (Bomphrey et al., 2017), but differ substantially from those of most other insect flyers that operate at much higher stroke amplitudes and correspondingly lower wingbeat frequencies (Alexander, 2004; Dudley, 2002). For example, a fruit fly of comparable mass beats its wings at an amplitude of 160 deg and frequency of 190 Hz (Muijres et al., 2014), which are four times and one-third the values for mosquitoes, respectively. The simple stroke-amplitude-based method that our mosquitoes use to increase force production when carrying a load is also very different from that of other flying insects and vertebrates, which exhibit more complex kinematic adjustments to increase force production, including changes in stroke amplitude, wingbeat frequency and angle of attack (Alexander, 2004; Dudley, 2002; Muijres et al., 2014). By contrast, honeybees, which carry large nectar and pollen loads, use kinematic patterns similar to those of mosquitoes, with high operating frequencies and low amplitudes, and also alter only stroke amplitude to adjust aerodynamic force production (Altshuler et al., 2005). Honeybee flight is aerodynamically less efficient (higher aerodynamic power costs) than that of fruit flies (Altshuler et al., 2005), and thus the low-amplitude wingbeats of mosquitoes might similarly be energetically suboptimal in normal hovering. Instead, the low-amplitude flight style used by mosquitoes and honeybees enables sustained flight with substantial loads by only increasing stroke amplitude, thereby allowing the insects to continue operating at the natural frequency of the oscillatory neuro-mechanical system (Pringle, 1957). In contrast, flyers that use high-amplitude wingbeats have no such capacity because stroke amplitude is anatomically limited to 180 deg, at which point the left and right wings collide at the end of each stroke (Lehmann and Dickinson, 1997).

Take-off speed and stealth in escaping malaria mosquitoes

We studied the voluntary and escape take-offs by blood-fed and unfed mosquitoes (Fig. 3). Compared with unfed individuals,

blood-fed mosquitoes on average had take-off speeds that were 18% lower, and ascent angles that were 28% lower than those of unfed mosquitoes (Fig. 3G,H, Table S2). A reduction in the escape speed of mosquitoes when carrying a blood load increases the risk of being captured by jumping spiders (Roitberg et al., 2003), and likewise might make mosquitoes more vulnerable to being killed by a host.

If slow take-offs increase the risk of being killed by a host, mosquitoes should perform faster take-offs when escaping from a vibratory stimulus than when performing a voluntary take-off, as is the case in fruit flies responding to looming stimuli (Card and Dickinson, 2008a). But surprisingly, we found no significant differences between voluntary and escape take-offs (Table S1). Our vibratory stimulus may have been insufficient to trigger escape dynamics, but the mosquitoes did respond robustly to the stimulus. In addition, the apparent inability of mosquitoes to perform the specialized escape take-offs that have been described in fruit flies (Card and Dickinson, 2008b) is also supported anatomically by leg muscle reconstructions (Figs 1D, 5). The extracoxal depressor of the trochanter of the middle mosquito leg is much smaller than that of the fruit fly and does not attach to the tergal/dorsal side of the thorax. Thus, as in tsetse flies, mosquitoes lack a TDT muscle specialized for performing rapid and forceful leg extensions required for powerful leg push-offs (King, 1983).

The fact that mosquitoes never evolved a specialized TDT muscle might be because mechanical constraints of long slender legs prevent mosquitoes from performing high-speed take-offs, or that the selection pressure for a fast escape take-off was not sufficiently strong. However, the chance of survival in mosquitoes escaping from jumping spiders correlates positively with take-off speed (Roitberg et al., 2003), suggesting that successful evasion from predators, and possibly irritated hosts, requires fast take-offs. We therefore interpret the absence of more robust legs with specialized TDT muscles in mosquitoes, and the consequent inability to perform rapid take-offs, as the result of a trade-off between escape speed and stealth. When taking off from a host, blood-feeding insects need to simultaneously maximize escape speed and minimize pressure forces exerted on the host, which are conflicting requirements.

To test this notion, we compared the take-off dynamics between malaria mosquitoes that must escape from a host with those of similarly sized fruit flies (Card and Dickinson, 2008a). Lift-off speeds in our mosquitoes are strikingly similar to those of fruit flies performing a voluntary take-off (mosquitoes: $U_{\text{lift-off}}=0.23\pm 0.05\text{ m s}^{-1}$, $n=63$; fruit flies: $U_{\text{lift-off}}=0.24\text{ m s}^{-1}$; Card and Dickinson, 2008a). In contrast, the weight-normalized peak push-off forces produced by mosquitoes were only 27% of those of fruit flies (mosquitoes: $F/mg_{\text{max}}=2.23\pm 0.47$, $n=63$; fruit flies: $F/mg_{\text{max}}=8.27$). Thus, mosquitoes are capable of reaching take-off speeds comparable to those of fruit flies, but with much lower push-off forces, which might possibly reduce the chance of being detected by the host. Mosquitoes achieve this by fully extending their relatively long legs throughout the push-off phase, allowing them to travel on average 88% of their body length away from the substratum while continuing to push off with their legs ($X_{\text{lift-off}}/l_{\text{body}}=0.88\pm 0.37$, $n=63$; Fig. 2, Movies 1–4); fruit flies, with their much shorter legs, travel only 25% of their body length during push-off (Card and Dickinson, 2008a). This process also extends the leg push-off duration in mosquitoes to 4.8 times the push-off duration of fruit flies (mosquitoes: $\Delta t_{\text{push-off}}=26.3\pm 11.5\text{ ms}$, $n=63$; fruit flies: $\Delta t_{\text{push-off}}=5.5\text{ ms}$). Because lift-off speed depends directly on the change in momentum during the push-off phase (Eqn 10), a longer push-off duration allows the mosquito to reach lift-off speeds similar to those

of fruit flies, despite much lower peak forces imposed on the substratum.

Because the vertebrate integument is highly sensitive to imposed pressures (Li et al., 2011), leg push-off forces with their imposed point loads can be more easily detected than the much more broadly distributed pressure waves produced by flapping wings (Anderson, 1991; Lentink et al., 2015). Mosquitoes thus further reduce the chance of being detected by having wings produce 61% of the force during push-off (Fig. 4, Table S4), rather than relying solely on forces generated by the legs pushing on the host, as is the case for escaping fruit flies (Card and Dickinson, 2008b). As a result, blood-fed mosquitoes produce peak leg forces ($F_{\text{leg,max}} \sim 0.02$ mN) that were below the detection threshold of mechanosensory hairs of mammals (0.07 mN; Li et al., 2011), whereas peak leg force of escaping fruit flies ($F_{\text{leg,max}} \sim 0.15$ mN) were above this threshold.

Thus, mosquitoes that escape from a host after blood feeding can achieve relatively high take-off speeds while generating peak forces imposed on the host that are below the detection threshold, despite the fact that they need to carry a blood meal that can double to triple the animals' total weight. Mosquitoes achieve this using wing-generated aerodynamic forces during push-off rather than relying just on forces produced by the legs, and by carrying out a precisely controlled extension of their relatively long legs. Reduction in tactile detection by the host following a blood meal, and possibly during landings, may be a general locomotor feature of blood-feeding insects.

Acknowledgements

We thank Tessa van den Bemt, Uros Cerkenvenik, Sander Gussekloo, Aron Kuiper, Martin Lankheet, Johan van Leeuwen, Remco Pieters and Henk Schipper for their help and valuable input. Léon Wester, Frans van Aggelen and André Gidding are acknowledged for rearing the mosquitoes.

Competing interests

The authors declare no competing or financial interests.

Author contributions

Conceptualization: F.T.M., S.W.C., W.G.v.V., J.S., B.T.B., M.A.K., R.D.; Methodology: F.T.M., W.G.v.V., J.S., B.T.B., M.A.K.; Software: F.T.M., W.G.v.V., B.T.B.; Validation: F.T.M., W.G.v.V.; Formal analysis: F.T.M., S.W.C., B.T.B.; Investigation: F.T.M., S.W.C., B.T.B.; Resources: F.T.M., J.S., M.A.K., R.D.; Data curation: F.T.M., S.W.C.; Writing - original draft: F.T.M.; Writing - review & editing: F.T.M., S.W.C., W.G.v.V., J.S., B.T.B., M.A.K., R.D.; Visualization: F.T.M.; Supervision: F.T.M., M.A.K., R.D.; Project administration: F.T.M., M.A.K., R.D.; Funding acquisition: F.T.M., M.A.K., R.D.

Funding

This work was supported by grants from the Netherlands Organization for Scientific Research (Nederlandse Organisatie voor Wetenschappelijk Onderzoek) [NWO-VENI-863-14-007 to F.T.M.], the National Science Foundation [DGE-0903711 to M.A.R.K. and R.D.] and the Wageningen Institute of Animal Sciences [visiting research fellow grant to S.W.C.]. The high-speed cameras were co-financed by Shared Research Facilities of Wageningen University & Research.

Data availability

Databases S1 to S3 are available from the Dryad Digital Repository (Muijres et al., 2017): <http://dx.doi.org/10.5061/dryad.1b312>.

Supplementary information

Supplementary information available online at <http://jeb.biologists.org/lookup/doi/10.1242/jeb.163402.supplemental>

References

- Alexander, D. E. (2004). *Nature's Flyers: Birds, Insects, and the Biomechanics of Flight*. Baltimore, MD: Johns Hopkins University Press.
- Altschuler, D. L., Dickson, W. B., Vance, J. T., Roberts, S. P. P. and Dickinson, M. H. (2005). Short-amplitude high-frequency wing strokes determine the aerodynamics of honeybee flight. *Proc. Natl. Acad. Sci. USA* **102**, 18213-18218.
- Anderson, J. D. (1991). *Fundamentals of Aerodynamics*, Vol. 1984. New York: McGraw-Hill.
- Bomphrey, R. J., Nakata, T., Phillips, N. and Walker, S. M. (2017). Smart wing rotation and trailing-edge vortices enable high frequency mosquito flight. *Nature* **544**, 92-95.
- Card, G. and Dickinson, M. H. (2008a). Performance trade-offs in the flight initiation of *Drosophila*. *J. Exp. Biol.* **211**, 341-353.
- Card, G. and Dickinson, M. H. (2008b). Visually mediated motor planning in the escape response of *Drosophila*. *Curr. Biol.* **18**, 1300-1307.
- Cignoni, P., Callieri, M., Corsini, M., Dellepiane, M., Ganovelli, F. and Ranzuglia, G. (2008). MeshLab: an Open-Source Mesh Processing Tool. In Sixth Eurographics Italian Chapter Conference, pp. 129-136. doi.org/10.2312/LocalChapterEvents/ItalChap/ItalianChapConf2008/129-136.
- Clements, A. N. (2011). The biology of mosquitoes. *Biol. Mosquitoes* **3**, 1-571.
- Dickinson, M. H. and Muijres, F. T. (2016). The aerodynamics and control of free flight maneuvers in *Drosophila*. *Philos. Trans. R. Soc. Lond. B Biol. Sci.* **371**, 20150388.
- Dudley, R. (2002). *The Biomechanics of Insect Flight: Form, Function, Evolution*. Princeton, NJ: Princeton University Press.
- Ellington, C. P. (1984). The aerodynamics of hovering insect flight. V. A vortex theory. *Phil. Trans. R. Soc. Lond. B Biol. Sci.* **305**, 115-144.
- Fontaine, E. I., Zabala, F., Dickinson, M. H. and Burdick, J. W. (2009). Wing and body motion during flight initiation in *Drosophila* revealed by automated visual tracking. *J. Exp. Biol.* **212**, 1307-1323.
- Hatze, H. (1988). High-precision three-dimensional photogrammetric calibration and object space reconstruction using a modified DLT-approach. *J. Biomech.* **21**, 533-538.
- King, D. G. (1983). Evolutionary loss of a neural pathway from the nervous system of a fly (*Glossina morsitans*/Diptera). *J. Morph.* **175**, 27-32.
- Krenn, H. W. and Aspöck, H. (2012). Form, function and evolution of the mouthparts of blood-feeding Arthropoda. *Arthropod. Struct. Dev.* **41**, 101-118.
- Lehmann, F.-O. and Dickinson, M. H. (1997). The changes in power requirements and muscle efficiency during elevated force production in the fruit fly *Drosophila melanogaster*. *J. Exp. Biol.* **200**, 1133-1143.
- Lentink, D., Haselsteiner, A. F. and Ingersoll, R. (2015). In vivo recording of aerodynamic force with an aerodynamic force platform: from drones to birds. *J. R. Soc. Interface* **12**, 20141283.
- Li, L., Rutlin, M., Abreira, V. E., Cassidy, C., Kus, L., Gong, S., Jankowski, M. P., Luo, W., Heintz, N., Koerber, H. R. et al. (2011). The functional organization of cutaneous low-threshold mechanosensory neurons. *Cell* **147**, 1615-1627.
- Metscher, B. D. (2009). MicroCT for comparative morphology: simple staining methods allow high-contrast 3D imaging of diverse non-mineralized animal tissues. *BMC Physiol.* **9**, 11.
- Mogil, J. S., Wilson, S. G. and Wan, Y. (2001). Assessing nociception in murine subjects. In *Methods in Pain Research* (ed. L. Kruger), pp. 11-40. Boca Raton, FL: CRC Press.
- Muijres, F. T., Elzinga, M. J., Melis, J. M. and Dickinson, M. H. (2014). Flies evade looming targets by executing rapid visually directed banked turns. *Science* **344**, 172-177.
- Muijres, F. T., Chang, S. W., van Veen, W. G., Spitzen, J., Biemans, B. T., Koehl, M. A. R. and Dudley, R. (2017). Data from: Escaping blood-fed malaria mosquitoes minimize tactile detection without compromising on take-off speed. Dryad Digital Repository. <http://dx.doi.org/10.5061/dryad.1b312>
- Pringle, J. (1957). *Insect Flight. Cambridge Monographs in Experimental Biology*, Vol. 9. Cambridge, UK: Cambridge University Press.
- Roitberg, B. D., Mondor, E. B. and Tyerman, J. G. A. (2003). Pouncing spider, flying mosquito: blood acquisition increases predation risk in mosquitoes. *Behav. Ecol.* **14**, 736-740.
- Sane, S. P. and Dickinson, M. H. (2002). The aerodynamic effects of wing rotation and a revised quasi-steady model of flapping flight. *J. Exp. Biol.* **205**, 1087-1096.
- Stampanoni, M., Marone, F., Modregger, P., Pinzer, B., Thüning, T., Vila-Comamala, J., David, C. and Mokso, R. (2010). Tomographic hard x-ray phase contrast micro- and nano-imaging at TOMCAT. *AIP Conf. Proc.* **1266**, 13-17.
- Takken, W. (1991). The role of olfaction in host-seeking of mosquitoes: a review. *Int. J. Trop. Insect Sci.* **12**, 287-295.
- Takken, W. and Knols, B. G. J. (1999). Odor-mediated behavior of Afrotropical malaria mosquitoes. *Annu. Rev. Entomol.* **44**, 131-157.

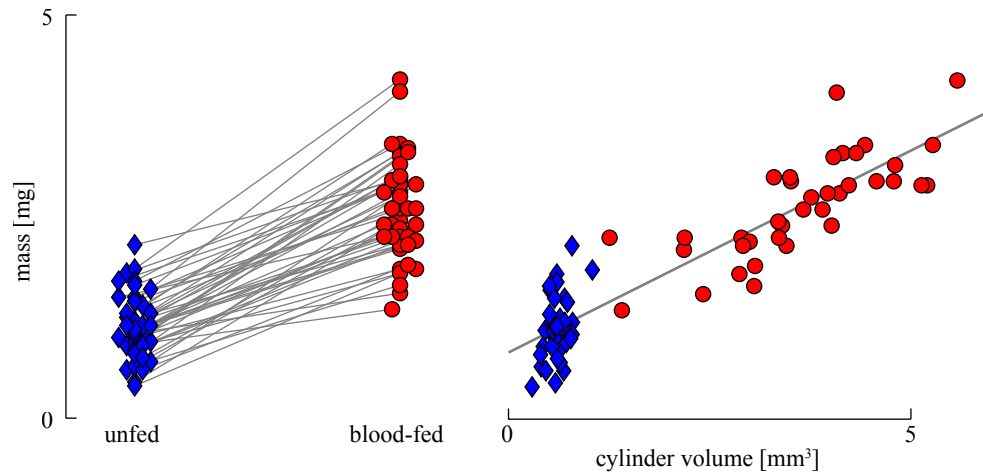


Fig. S1. Body mass was estimated based on the size of the mosquito, expressed by the cylindrical volume metric (Eqn. 1). (A) mass of all 44 measured mosquitoes before and after blood feeding. (B) correlation between body mass and the cylindrical volume metric for all mosquitoes, as described by the grey trend line (Eqn. 2). In both panels, blue diamonds are for mosquitoes before blood feeding, and red circles refer to post-blood feeding.

Table S1. Incentive (voluntary take-off or substrate vibration stimulus) did not significantly affect kinematics or force production during the take-off.

parameter	condition	incentive	n	mean	standard deviation	median	Q1	Q3	normality p-value	incentive p-value
Mass ratio (Rm) [-]	unfed	voluntary	15	1.01	0.05	1.00	0.97	1.04	0.908	0.737
		stimulus	16	0.99	0.08	1.01	0.95	1.01	0.812	
	blood-fed	voluntary	17	1.92	0.35	1.85	1.78	1.97	<0.001	0.406
		stimulus	15	1.95	0.28	1.90	1.79	2.12	0.868	
Push-off time ($\Delta t_{\text{push-off}}$) [ms]	unfed	voluntary	15	26.0	11.4	22.1	20.9	26.9	<0.001	0.953
		stimulus	16	26.5	11.9	22.6	19.3	28.7	0.001	
	blood-fed	voluntary	17	37.5	17.0	30.1	25.8	42.3	0.005	0.113
		stimulus	15	28.7	8.1	29.0	23.2	30.8	0.055	
Lift-off displacement ($X_{\text{lift-off}}/l_{\text{body}}$) [-]	unfed	voluntary	15	0.94	0.51	0.73	0.68	1.07	<0.001	0.441
		stimulus	16	0.78	0.28	0.73	0.61	0.88	<0.001	
	blood-fed	voluntary	17	0.99	0.32	0.92	0.86	1.06	0.024	0.054
		stimulus	15	0.80	0.33	0.76	0.57	0.93	0.095	
Lift-off speed ($U_{\text{lift-off}}$) [m s^{-1}]	unfed	voluntary	15	0.26	0.06	0.25	0.23	0.30	0.835	0.464
		stimulus	16	0.24	0.04	0.25	0.20	0.27	0.766	
	blood-fed	voluntary	17	0.21	0.04	0.22	0.18	0.23	0.200	0.122
		stimulus	15	0.19	0.06	0.18	0.15	0.22	0.371	
Lift-off ascent angle ($\gamma_{\text{lift-off}}$) [-]	unfed	voluntary	15	48°	12°	51°	43°	58°	0.028	0.540
		stimulus	16	52°	21°	55°	32°	70°	0.552	
	blood-fed	voluntary	17	34°	25°	40°	7°	54°	0.061	0.650
		stimulus	15	39°	23°	39°	22°	56°	0.927	
Lift-off body pitch ($\beta_{\text{lift-off}}$) [-]	unfed	voluntary	15	13°	18°	17°	4°	29°	0.131	0.890
		stimulus	16	13°	20°	21°	-4°	29°	0.315	
	blood-fed	voluntary	17	25°	13°	29°	20°	33°	0.001	1.000
		stimulus	15	25°	15°	25°	17°	38°	0.610	
Push-off force ($F/mg_{\text{push-off}}$) [-]	unfed	voluntary	15	2.08	0.40	2.06	1.87	2.29	0.423	0.395
		stimulus	16	1.98	0.46	1.94	1.71	2.23	0.605	
	blood-fed	voluntary	17	1.54	0.30	1.64	1.21	1.77	0.030	0.850
		stimulus	15	1.58	0.26	1.50	1.39	1.82	0.775	
Maximum push-off force ($F/mg_{\text{push-off}}$) [-]	unfed	voluntary	15	2.43	0.43	2.44	2.18	2.70	0.919	0.828
		stimulus	16	2.48	0.44	2.41	2.24	2.61	0.152	
	blood-fed	voluntary	17	2.00	0.45	2.14	1.62	2.34	0.169	0.910
		stimulus	15	2.03	0.36	2.06	1.81	2.24	0.297	
Aerial flight speed (U_{aerial}) [m s^{-1}]	unfed	voluntary	15	0.34	0.09	0.35	0.25	0.42	0.376	0.395
		stimulus	16	0.37	0.11	0.37	0.28	0.46	0.988	
	blood-fed	voluntary	17	0.36	0.07	0.39	0.30	0.40	0.368	0.308
		stimulus	15	0.34	0.08	0.32	0.27	0.41	0.177	
Aerial ascent angle (γ_{aerial}) [-]	unfed	voluntary	15	30°	16°	36°	25°	42°	0.026	0.093
		stimulus	16	21°	21°	24°	1°	33°	0.634	
	blood-fed	voluntary	17	17°	17°	17°	6°	29°	0.971	0.546
		stimulus	15	13°	22°	-2°	-4°	35°	0.006	
Aerial body pitch (β_{aerial}) [-]	unfed	voluntary	15	26°	24°	39°	12°	43°	0.038	0.243
		stimulus	16	20°	20°	26°	1°	34°	0.028	
	blood-fed	voluntary	17	31°	15°	33°	27°	42°	0.037	0.571
		stimulus	15	28°	18°	29°	13°	45°	0.341	
Aerial force (F/mg_{aerial}) [-]	unfed	voluntary	15	1.05	0.11	1.03	0.98	1.10	0.827	0.859
		stimulus	16	1.06	0.15	1.02	0.98	1.10	0.039	
	blood-fed	voluntary	17	1.10	0.11	1.12	1.01	1.14	0.219	0.910
		stimulus	15	1.03	0.09	1.05	1.00	1.09	0.109	

Table S2. The effect of blood-feeding on body mass, and on the take-off dynamics and force production throughout the complete take-off.

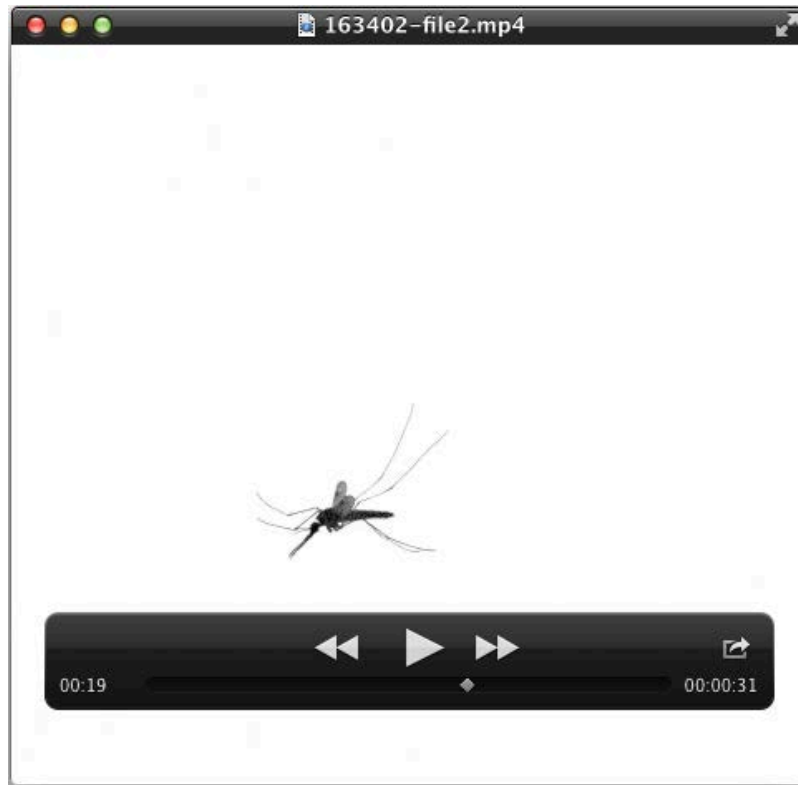
parameter	feeding condition	n	mean	standard deviation	median	Q1	Q3	normality p-value	feeding condition p-value
Mass ratio (R_m) [-]	unfed	31	1.00	0.06	1.01	0.97	1.04	0.867	0.010
	blood-fed	32	1.93	0.32	1.88	1.80	2.02	< 0.001	
Push-off time ($\Delta t_{\text{push-off}}$) [ms]	unfed	31	26.3	11.5	22.6	19.6	27.4	< 0.001	0.002
	blood-fed	32	33.4	14.1	29.3	25.3	36.4	< 0.001	
	all	63	29.9	13.3	26.0	21.3	32.2	-	-
Lift-off displacement ($X_{\text{lift-off}}/l_{\text{body}}$) [-]	unfed	31	0.86	0.41	0.73	0.65	0.89	< 0.001	0.159
	blood-fed	32	0.90	0.33	0.89	0.69	0.98	0.023	
	all	63	0.88	0.37	0.80	0.67	0.93	-	-
Lift-off speed ($U_{\text{lift-off}}$) [m s ⁻¹]	unfed	31	0.25	0.05	0.25	0.21	0.28	0.454	0.001
	blood-fed	32	0.20	0.05	0.21	0.16	0.23	0.500	
	all	63	0.23	0.05	0.23	0.19	0.26	-	-
Lift-off ascent angle ($\gamma_{\text{lift-off}}$) [-]	unfed	31	50°	17°	53°	35°	60°	0.493	0.016
	blood-fed	32	36°	24°	39°	15°	55°	0.221	
Lift-off body pitch ($\beta_{\text{lift-off}}$) [-]	unfed	31	13°	19°	19°	-2°	29°	0.045	0.010
	blood-fed	32	25°	14°	28°	18°	34°	0.026	
Push-off force ($F/mg_{\text{push-off}}$) [-]	unfed	31	2.03	0.43	1.97	1.75	2.29	0.277	0.008
	blood-fed	32	1.56	0.28	1.57	1.37	1.77	0.049	
Maximum push-off force ($F/mg_{\text{push-off, max}}$) [-]	unfed	31	2.46	0.43	2.44	2.21	2.63	0.249	0.030
	blood-fed	32	2.01	0.41	2.10	1.71	2.27	0.160	
	all	63	2.23	0.47	2.23	2.01	2.48	-	-
Aerial flight speed (U_{aerial}) [m s ⁻¹]	unfed	31	0.36	0.10	0.36	0.27	0.43	0.953	0.853
	blood-fed	32	0.35	0.07	0.35	0.29	0.41	0.133	
Aerial ascent angle (γ_{aerial}) [-]	unfed	31	26°	19°	31°	9°	40°	0.134	0.035
	blood-fed	32	15°	19°	12°	-3°	30°	0.064	
Aerial body pitch (β_{aerial}) [-]	unfed	31	23°	22°	27°	6°	40°	0.013	0.219
	blood-fed	32	30°	16°	32°	22°	44°	0.040	
Aerial force (F/mg_{aerial}) [-]	unfed	31	1.05	0.13	1.03	0.98	1.10	0.033	0.251
	blood-fed	32	1.07	0.10	1.08	1.00	1.13	0.136	

Table S3. The effect of blood-feeding on wingbeat kinematics during the aerial phase of the take-off.

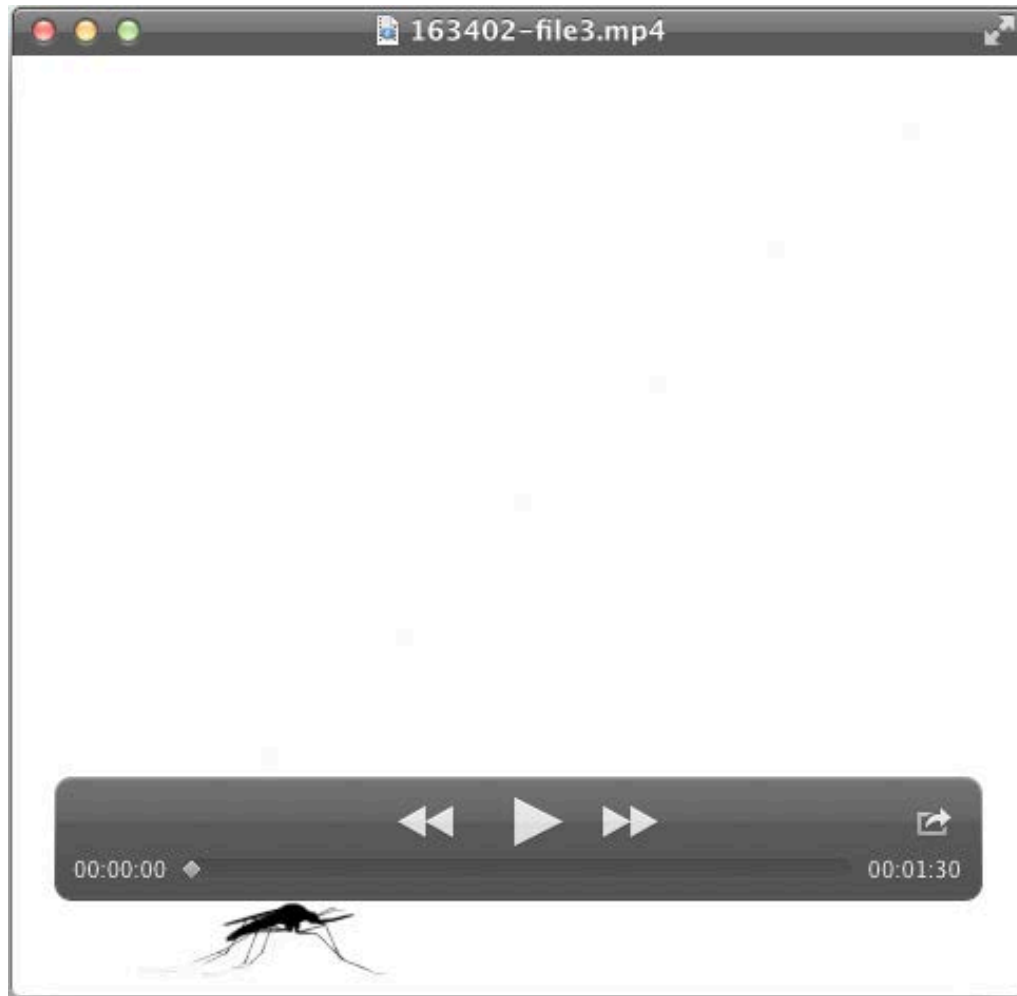
parameter	feeding condition	n	mean	standard deviation	median	Q1	Q3	normality <i>p</i> -value	feeding condition <i>p</i> -value
Wingbeat frequency (<i>f</i>) [Hz]	unfed	29	579	38	584	555	603	0.505	0.534
	blood-fed	29	573	37	582	543	594	0.635	
Stroke amplitude (A_{stroke}) [-]	unfed	29	42°	5°	42°	39°	46°	0.473	<0.001
	blood-fed	29	54°	6°	56°	50°	59°	0.268	
Pitch amplitude (A_{pitch}) [-]	unfed	29	121°	10°	122°	114°	129°	0.692	<0.001
	blood-fed	29	134°	12°	135°	124°	139°	0.614	
Stroke-plane pitch adjustment (σ) [-]	unfed	29	-1°	4°	-1°	-4°	1°	0.221	<0.001
	blood-fed	29	-9°	4°	-9°	-12°	-5°	0.130	

Table S4. The relative contribution of leg-derived push-off forces and wing-derived aerodynamic forces to total force production during the push-off phase and aerial phase of the take-off.

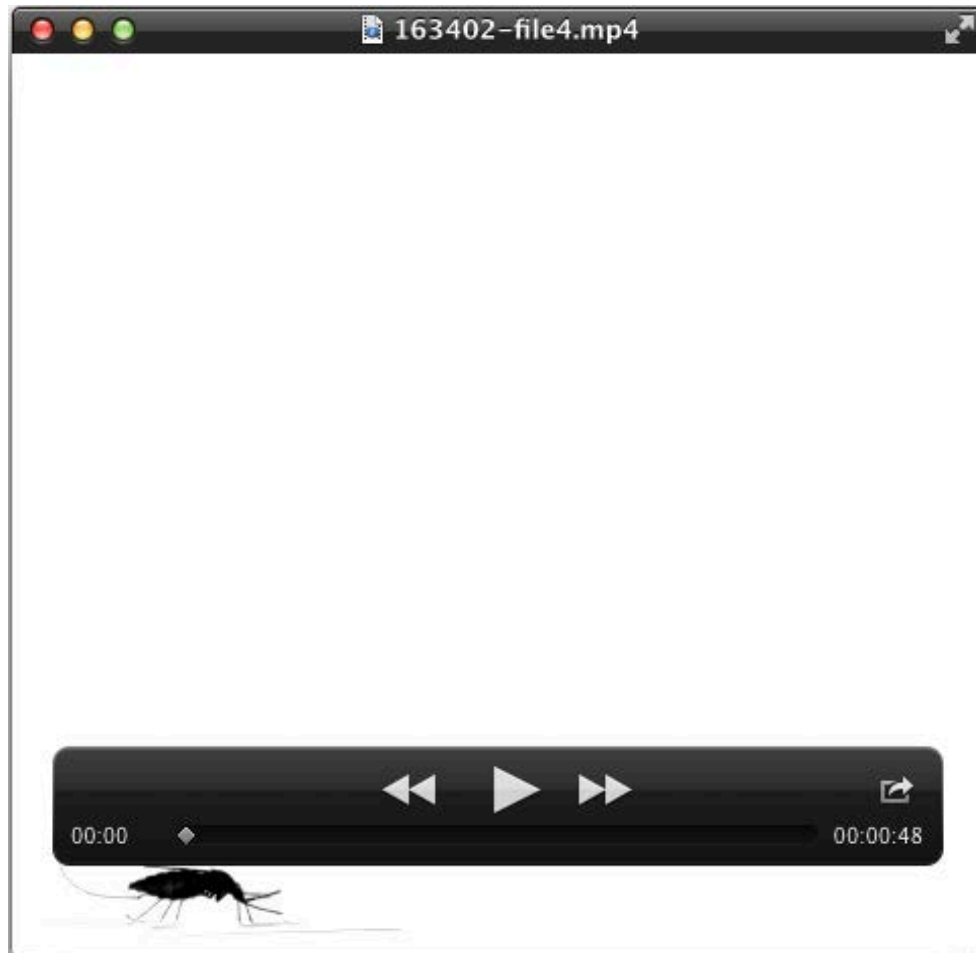
parameter	feeding condition	n	mean	standard deviation	median	Q1	Q3	normality <i>p</i> -value	feeding condition <i>p</i> -value
Push-off force ($F/mg_{\text{push-off}}$) [-]	total force	16	2.04	0.41	1.92	1.75	2.36	0.236	<0.001
	aerodynamic	16	1.13	0.42	0.98	0.83	1.39	0.066	
Aerial force (F/mg_{aerial}) [-]	total force	16	1.18	0.19	1.17	1.00	1.39	0.093	0.136
	aerodynamic	16	1.14	0.41	1.05	0.87	1.18	<0.001	
Force ratio ($F_{\text{aero}}/F_{\text{leg}}$) [-]	unfed	8	2.13	1.64	1.70	1.00	3.00	0.086	0.105
	blood-fed	8	0.96	0.24	0.91	0.76	1.20	0.269	
	all	16	1.55	1.29	1.20	0.76	1.71	-	



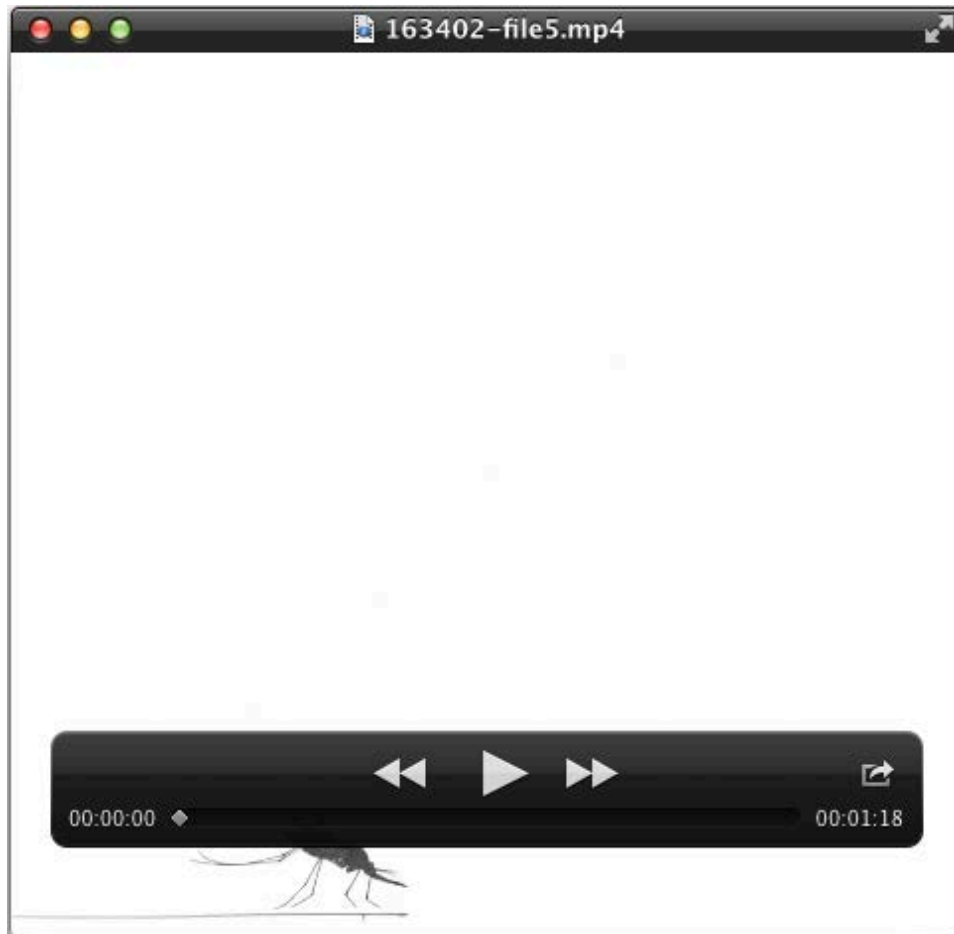
Movie 1. High-speed video of the take-off of an unfed mosquito filmed from the side. The video was recorded at 13,500 frames per second, and play-back was slowed down 450 times. The video corresponds to the photo-montage of Fig. 2A.



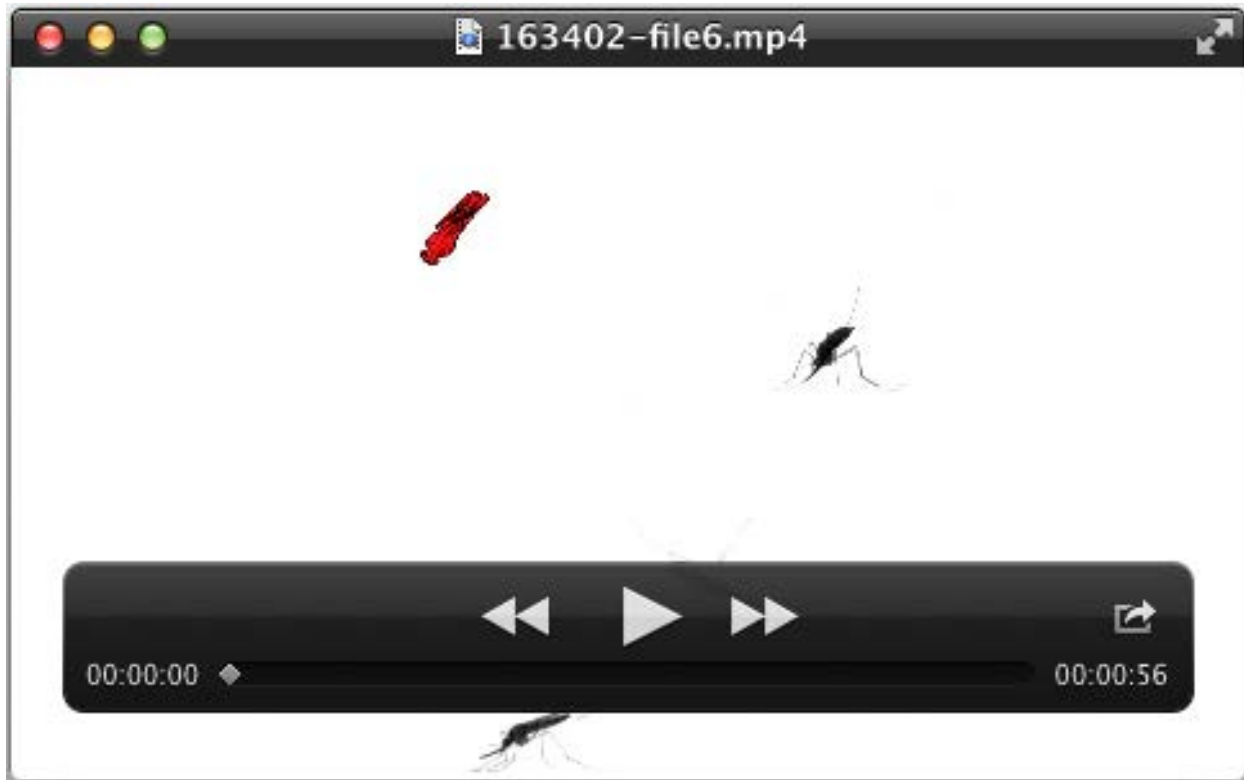
Movie 2. High-speed video of the take-off of an unfed mosquito filmed from the side. The video was recorded at 13,500 frames per second, and play-back was slowed down 450 times. The video corresponds to the photo-montage of Fig. 2B.



Movie 3. High-speed video of the take-off of a blood-fed mosquito filmed from the side. The video was recorded at 13,500 frames per second, and play-back was slowed down 450 times. The video corresponds to the photo-montage of Fig. 2C.



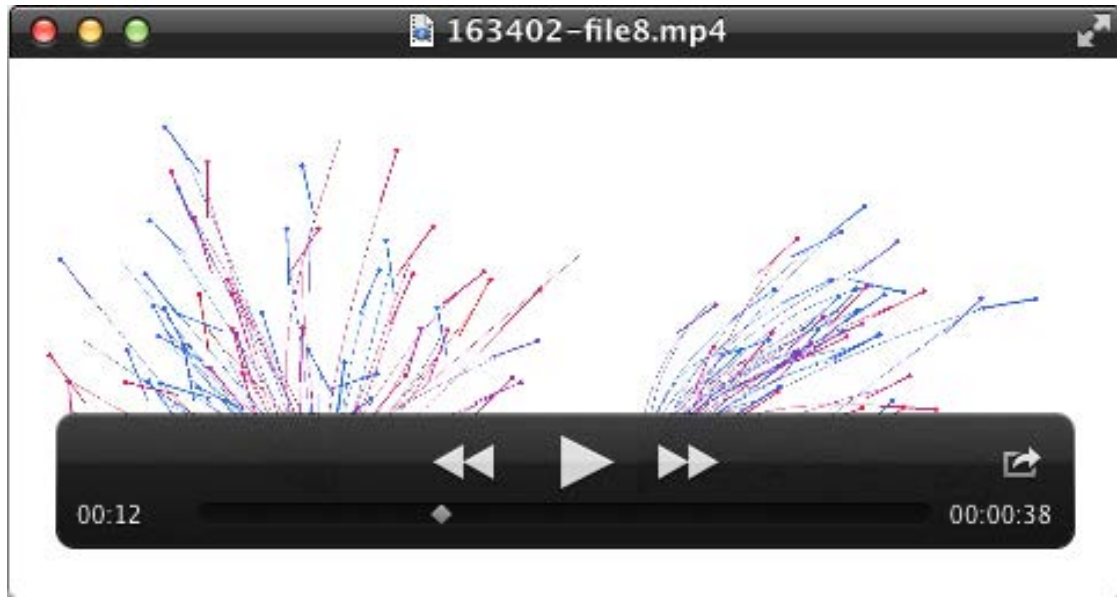
Movie 4. High-speed video of the take-off of a blood-fed mosquito filmed from the side. The video was recorded at 13,500 frames per second, and play-back was slowed down 450 times. The video corresponds to the photo-montage of Fig. 2D.



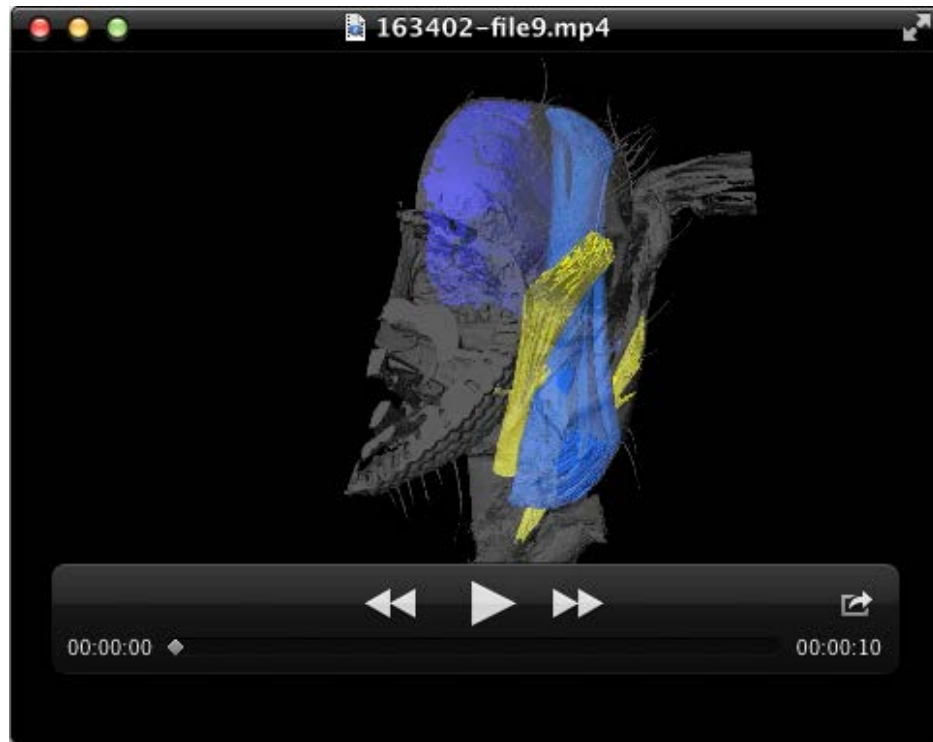
Movie 5. High-speed video and 3D model reconstruction from video tracking for the unfed mosquito of Fig. 5A-D. The movie consists of the front view video (top right), side view video (bottom left), top view video (bottom right), and the 3D model reconstruction (top left). The mosquito model consists of a rigid body and two rigid wings. The videos were recorded at 13,500 frames per second, and play-back was slowed down 450 times.



Movie 6. High-speed video and 3D model reconstruction from video tracking for the blood-fed mosquito of Fig. 5F-I. The movie consists of the two perpendicular side view videos (top right and bottom left), top view video (bottom right), and the 3D model reconstruction (top left). The mosquito model consists of a rigid body and two rigid wings. The videos were recorded at 13,500 frames per second, and play-back was slowed down 450 times.



Movie 7. Top view (left) and side view (right) of the take-off dynamics of all experimental mosquitoes, corresponding to Fig. 3A,B. The trajectories were overlaid such that all lift-offs occurred at the same time. Thin lines show flight trajectories, and lollypops show the orientation of the longitudinal body axis, whereby the circles indicate head position, and stick length represents body length. The take-off dynamics is slowed down 100 times. Trajectories are color-coded with body weight according to the color-bar in Fig. 3B.



Movie 8. Three-dimensional μ CT reconstruction of the muscular system within the left half of the thorax of a female malaria mosquito, as also shown in Fig. 6. The indirect flight power muscles consist of the dorso-ventral muscles (in light blue) and the dorso-longitudinal muscles (in dark blue). The leg muscles that mostly power push-off are the extracoxal depressor muscles of the trochanter of the front, middle and hind leg (in yellow). Surrounding material that was stained but did not belong to the segmented muscles was visualized in transparent grey.